Journal Name

ARTICLE TYPE

Cite this: DOI: 10.1039/xxxxxxxxxx

Recent Advances in the Biomimicry of Structural Colours

Ahu Gümrah Dumanli[a] and Thierry Savin[b]

Received Date
Accepted Date

DOI: 10.1039/xxxxxxxxxx

www.rsc.org/journalname

Nature has mastered the construction of nanostructures with well-defined macroscopic effects and purposes. Structural colouration is a visible consequence of the particular patterning of a reflecting surface with regular structures at submicron length scales. Structural colours usually appear bright, shiny, iridescent or with a metallic look, as the result of physical processes such as diffraction, interference, or scattering with typically small dissipative loss. These features have recently attracted much research efforts in materials science, chemistry, engineering and physics, in order to understand and produce structural colours. In these early stages of photonics, researchers facing an infinite array of possible colour-producing structures are heavily inspired by the elaborated architectures they find in nature. We here review the recent technological strategies employed to artificially mimic the structural colours found in nature, as well as some of their current and potential applications.

1 Introduction

Colours play an essential role in the evolution and survival of plants and animals. To the best of our current knowledge, the colours of living creatures are produced either through pigments, bioluminescence, or spatial structures.[1] Pigmentary colours originate from the selective absorption of light by the electrons of molecules embedded in the materials. Bioluminescence is emitted by chemical reactions in the photophores of some organisms.[1,2] The third type of colouration is the result of the discrimination of wavelengths by the interaction of the incident light with structures on the reflective biomaterial. In the visible range of wavelengths, diffracting structures must be in the submicron scale in order to interact with light, and such patterns are indeed quite common in biological assemblies.[3]

These so-called "structural colours" usually have a distinctive appearance (shiny, metallic aspect with often an angle-dependent apparent colour) that contrasts with the dull and diffuse aspect of more common pigmentary colours. Physically, structural colours are the result of the fundamental optical processes of diffraction, interference or scattering. They generally suffer little dissipative loss,[4] and do not fade like pigments, which are sensitive to chemical alterations and have relatively low environmental resistance. In nature, these structures have been optimised, after millions of years of evolutionary trials and errors, to display the colouration most adapted to the various needs and purposes of living creatures, thus fulfilling important roles such as signalling (selection, advertising, etc.) or camouflage, for example.

Structural colours in nature have fascinated scientists for centuries, but their accurate assessment was only permitted by the introduction the scanning electron microscope (SEM) in the 1940's.[5] This discovery has triggered an extraordinary new perspective on the description and understanding of the natural nanostructures found in living matter, and indeed those responsible for colouration. As of today, a prodigious array of colour-producing architectures has been described by scientists in animals, plants and minerals, and new ones are still frequently discovered.

The engineering potentials of structural colours, for systematic usage in photonics (and possibly elsewhere), were first recognised about 30 years ago with the inception of the so-called "photonic crystals."[6] These materials can "mold the flow of light,"[7] in the manner that atomic crystals control the transport of electrons. Since then, intense research efforts have been carried out to overcome the two main and concomitant problems when building efficient photonic materials. First, how to best design the light-interfering structure for a given motive. Second, how to actually build these nanostructured materials. As with many other examples of recent technological advances, biomimicry is an elegant shortcut towards the optimisation of design.[8] For the second challenge, scientists already benefit from a strong footing to establish micromanufacturing methods for photonic materials.

Until about two decades ago, progress in microfabrication technologies were mainly driven by the microelectronic indus-

[a] Department of Chemistry, University of Cambridge, Lensfield Road, Cambridge CB2 1EW, United Kingdom.
[b] Department of Engineering, University of Cambridge, Trumpington Street, Cambridge CB2 1PZ, United Kingdom. E-mail: t.savin@eng.cam.ac.uk

try, which started in the 1950's with the invention of the integrated circuit. Microfabrication techniques are now employed to manufacture a plethora of miniaturized devices, with scopes well beyond pure electronics. In fact, the implementation of microdevices established entirely new disciplines, depending on the function sought (sensor, actuator, imaging, communication, mechanics, etc.), the materials used (silicon, metals, polymer, ceramics, etc.), and the fabrication processes employed (patterning, etching, moulding, deposition, etc.). Micro-electro-mechanical systems (MEMS), in particular, are recent applications of microfabrication that have been booming in recent years. They have driven many innovations in micro-machining, and are, today, found in mundane consumer products.[9]

As a result of these advances, submicron features can currently be fabricated with, generally, high throughput, and with a high degree of reproducibility. Although, building large assemblies, with the regular and periodic arrangements of microstructures required for photonic crystals, still remains a manufacturing challenge, particularly in three dimensions. The development of photonic nanomaterials, bio-inspired or custom-designed, may have now become the main driving force behind contemporary endeavours to push progress in microfabrication. These current efforts attract the interest of a large body of scientists, across many fields: chemistry, engineering, physics, materials science, biology, etc.

There already exists a vast literature on structural colouration and photonic materials, their incidence in nature, and their physical origins and underlying optical mechanisms. Consequently, recent years have seen the publication of many excellent review articles[1,3,4,8,10–24] and books[2,25–27] on these subjects. However, reviews covering the fabrication of bio-inspired photonic structures[28,29] are more rare, and do not specifically focus on the actual manufacturing techniques. We believe that the recent, and often remarkably ingenious, methods to reproduce natural structural colours deserve to be highlighted, and indeed have the potential to serve a wide spectrum of scientists.

This review thus puts a strong emphasis on microfabrication techniques. It is organised with a "what/how/why" outline, as follows: we first give a brief overview of the physical principles behind the structural colourations of some natural systems. In particular, we highlight four typical structures found in nature, representing the canonical systems, which, from our review of the latest literature, have attracted most studies in structural colour biomimicry. We next focus our attention on the recent techniques and attempts to mimicking the structural colours found in nature. We distinguish two main strategies, "top-down" and "bottom-up," as this splitting of technologies is quite general when presenting the routes for fabricating complex materials. The last part of our article is devoted to the most recent and promising applications of structural colours inspired by nature.

2 Natural Structural Colors

2.1 Physical origins of natural structural colours

The physical origins of structural colours have been summarised in several reviews.[2–4,10,11,18,19] In general terms, structural colours are produced by the microscopic patterns of a reflective material. Features with sizes comparable to the wavelength of the incident illumination diffract the light selectively to cause interference effects that can be constructive or destructive.[30] These interferences thus only allow ranges of wavelengths to be reflected and produce, when visible, a particular colouration of the material.[2] The range of reflected wavelength usually varies with the polarisation of the incident light. But more strikingly, it often depends strongly on the refracting angle, meaning that apparent colours change when varying the viewing orientation. Hence, structural colours often appear "iridescent."

To help understand in more details the design criteria underlying the production of structural colours, we first review the physical principles behind the processes generating these phenomena.[3,25] The relevant quantity to study is the reflectance of the medium at its interface with the exterior and for visible wavelengths between $400-700\,\mathrm{nm}$. The calculation of reflectance is performed using physical optics principles,[2,4,30,31] which can be categorised as diffraction gratings, films interference, photonic crystals and scattering.

A diffraction grating is a common occurrence of structural colouration (e.g. the reflection from a compact disc). It typically involves a single reflecting material, which displays on its surface a sub-wavelength pattern that is periodically repeated with a typical spacing d (Fig. 1B). The reflected spectrum will exhibit peaks located at a discrete set of wavelengths $\{\lambda_m\}_{m\in\mathbb{Z}}$, satisfying $m\lambda_m = d(\sin\theta_\mathrm{i} - \sin\theta_\mathrm{r})$ when observed at a reflective angle θ_r and for an incident light at an angle θ_i (both θ_r and θ_i are directions from the normal of the reflective plane, as shown in Fig. 1A). Contrary to the other structural colors, there is no separation of colours under specular reflection $\theta_\mathrm{r} = \theta_\mathrm{i}$. Examples of structural colours obtained from diffraction grating in nature include the floral iridescence,[32] butterfly scales,[33] or mollusc shells.[34]

Another simple structure that generates colour is a layered media, where thin films are stacked parallel to the reflecting interface (Fig. 1C and 1D). Layered media are very common in natural structural colours, and their fabrication based on thin-film deposition is routinely performed to produce optical components such as Bragg mirrors.[31,35] The reflected spectrum resulting from interference within the periodically stacked films (with period d) will again exhibit a set of resolved peaks at wavelengths λ_m that, approximately, follow the Bragg-Snell law:

$$m\lambda_m \approx 2d\sqrt{\bar{n}^2 - n_\mathrm{i}^2\sin^2\theta_\mathrm{i}}\,, \quad \text{with } m\in\mathbb{N}, \tag{1}$$

in an incident medium of refractive index n_i (typically $n_\mathrm{i}=1$ for air or $n_\mathrm{i}=1.33$ for water), and under specular reflection $\theta_\mathrm{r}=\theta_\mathrm{i}$ on the structured material with average, effective refractive index $\bar{n}$ ($\bar{n}$ may be calculated using the Maxwell-Garnett relation,[2] for example). This equation can also be used for the important case of helicoidal stacked polarising layers, similar to chiral nematic (or cholesteric) liquid crystals (see Fig. 7), which are common in nature. In that case, the chiral nematic half-pitch substitutes the periodicity of the stack.[36] In nature, thin film structural colours can be found, for example, in insect wings[37] or bird feathers.[38,39] Multilayer interference is very common in natural structural colours. They have been found and characterised in many

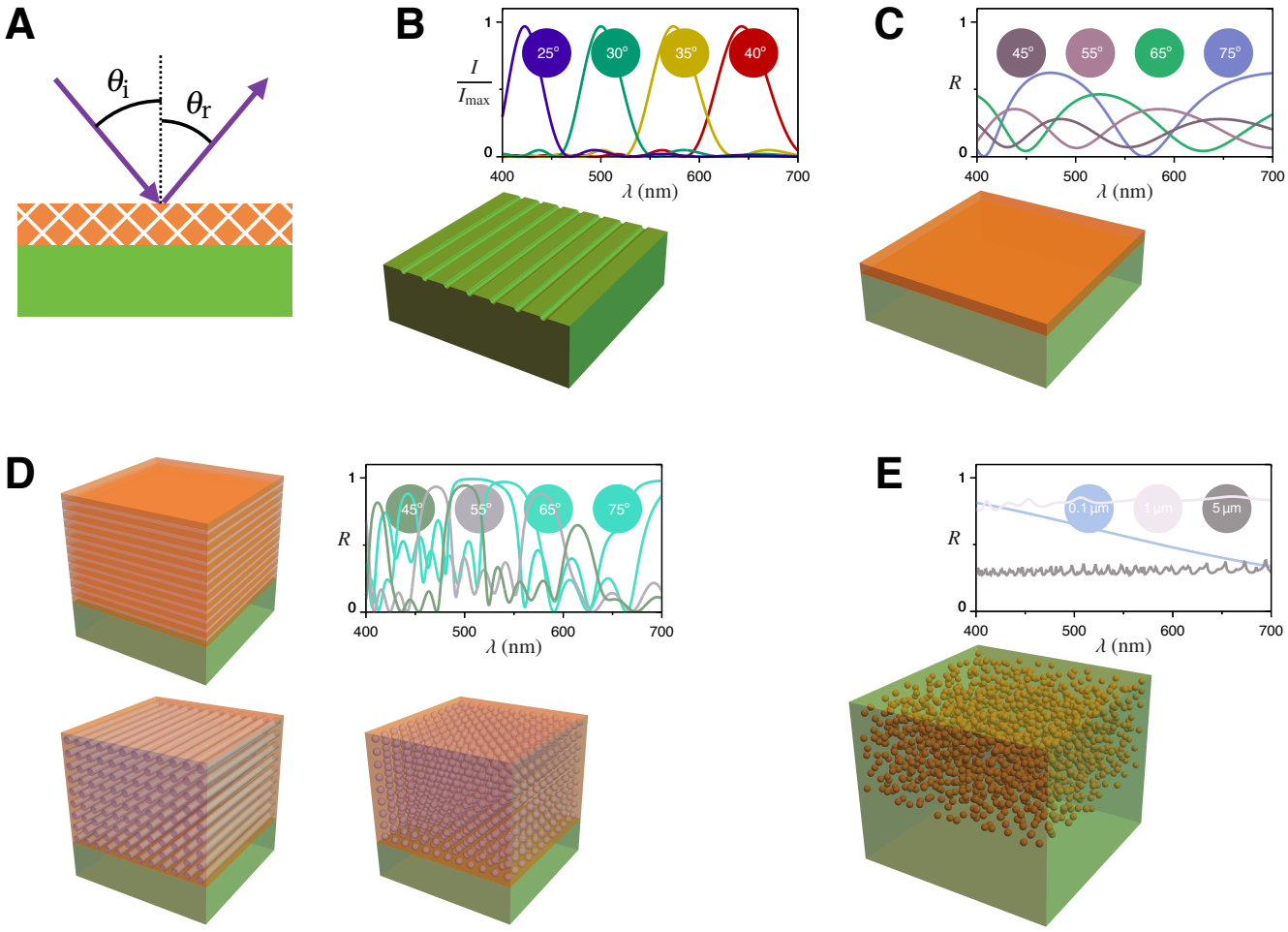

Fig. 1 (A) The reflectance of a colour-producing structure, in contact with the incident medium and supported by a substrate, must be assessed for given incidence and refraction angles, θ_i and θ_r, respectively; specular reflection is for $\theta_i = \theta_r$. (B) A reflective diffraction grating is obtained when a reflecting surface displays periodic patterns: here, parallel grooves are etched at regular intervals; the inset gives a typical spectrum of reflected intensity, showing angle-dependent wavelength discrimination. (C) Colouration can be obtained when a thin film of material is deposited on a substrate; the inset shows a corresponding example of reflectance spectrum at different angles of specular reflection. (D) One-, two- and three-dimensional (1D, 2D and 3D) photonic crystals have a structural periodicity in one, two, or three directions, respectively; in principle, photonic crystals are considered infinite, but in practice, they are bounded by a substrate and the exterior. 1D photonic crystals are multi-layers stacks, and the inset gives a typical spectrum of their reflectance. (E) Light scattered by a slab of a turbid material is also a kind of structural colour; for sufficently small scatterers, the reflected spectrum favors lower wavelengths (blue) as illustrated by the spectra shown in inset for various scatterers' sizes.

organisms, including insects,[40,41] birds,[42] fish,[43] mollusks[44,45] and fruits.[46]

Photonic crystals are materials having a spatially periodic refractive index, with the period near the wavelength of the incident light (Fig. 1D). In general, photonic crystals have dimensions much larger than their periodicity, so that they can be considered as infinite structures in calculations.[47–49] The periodicity can be only in one dimension, in which case the crystal is the periodic multilayer. The Bragg-Snell law, Eq. (1), can be used to evaluate the approximate set of reflectance peak wavelengths in a given direction of the crystalline lattice. In most cases, however, there are no simple calculations to evaluate the width of these peaks, or even their existence. The spectrum must generally be obtained via computational modelling relying on finite elements, plane-wave expansion, or finite-difference time-domain methods, to name a few. The focus of the calculations is to obtain the "photonic band-gaps" in their optical modes, that is the frequency ranges in which propagation of light is prohibited by the crystal. Band-gaps depend on the orientation of the propagation in the crystal, often quantified in the lattice reciprocal space, and correspond to iridescent reflectance peaks.[50] Natural two-dimensional photonic crystals provide the colouration of several marine animals[51] and birds.[52,53] Opals are archetypical of 3D photonic crystals,[54] which are also common in insects.[55–58]

Tunable structural colours from photonic crystals are used by some organisms for camouflage, predation, communication, etc.[3] These rely on varying the various parameters setting the peak's wavelength of reflectance in Eq. (1). Fudouzi[21], Zhao *et al.*[22] and Xu and Guo[24] recently proposed reviews of these mechanisms in nature and recent efforts in their biomimicry.

Light scattering is a fundamental process that describes the interactions of light with elementary particles of matter (scatterers). If the scatterers are spherical particles, it is often called Mie scattering, while the limit for small particle sizes, well below the

wavelength, is the Rayleigh scattering.[59] Light scattering is different from the processes previously described, although the laws of refraction are the results of the multiple light scattering events occurring in a bulk material. In this regard, a classification for the production of structural colour qualifies the mechanism as either coherent or incoherent. In coherent scattering, there is a phase relationship between the scattered waves by ordered scatterers and usually yields iridescence. Incoherent scattering is the result of disordered dispersion of scatterers, as shown in Fig. 1E, and has a diffuse appearance in reflection, with the spectrum independent of the observation or illumination angle (except in amplitude). Incoherent light scattering is at the origin of the white colour of milk, or the blue colour of the sky. An intermediate state of coherent, but non-iridescent scattering, has been observed where the scatterers are in fact quasi-ordered (or "weakly localised").[60] Light scattering produces the apparent colours of bird feathers,[61] Beetle scales,[62,63] or fishes,[64] for example.

Another way of producing colours via structure can be obtained with nano-patterned metallic films via their surface-plasmon resonance.[65] Since this mechanism is not observed in natural systems, it will not be specifically considered in this review.

Natural colour-producing assemblies often rely on a combinations of these canonical processes. For example, irregularity in the structure may also play a role in producing an additional diffusive appearance for the reflected light. And in some cases the optical processes are accompanied by large-scale structures to generate macroscopic effects on the colouration.[4] Moreover, natural materials' dispersion, adsorption or even birefringence can also convolute further the reflective response of color-producing structures (for example, by altering the polarisation of the reflected light). Intricate effects are also obtained via colour mixing, which is found in some living species. Hence, a structural colour may be associated with pigmentary colours (e.g., the *Margaritaria nobilis* fruit[66,67]), fluorescence (e.g., the *Troides magellanus* butterfly[68]), or another structural colour (e.g., *Entimus imperialis* weevil[69] or the *Papilio* butterfly[70,71]).[72]

Living organisms are the result of precise, multiscale and multifunctional arrangements of materials, from their molecular elements to their macroscopic shape, and structural colours epitomize this hierarchy.

2.2 Natural systems relevant for biomimicry

One of the most studied species, in terms of structural colour production and biomimetics, is the *Morpho* butterfly, whose wing-scales exhibit a unique metallic-blue colour. *Morpho* is an excellent example of the combined diversity of physical mechanisms in colour production (see Fig. 2A), hence all the more challenging to mimic. The iridescent blue colour with high reflectivity is a result of coherent scattering in the periodic arrays of scales.[75,76] Periodic structures, such as gratings or multilayers, produce colours with high dependency on the angle of reflection. However, for the *Morpho* species, the reflected blue colour has a low angle-dependency due to the presence of multilayer surfaces that exhibit a distribution of tilts with respect to the scales' substrate. The strong diffraction is further caused by a second layer of periodic ridges above the layer of highly iridescent ground.[77] As a result, *Morpho* butterfly wings exhibit a complex optical response by combining multilayer interference, diffraction, scattering, and even pigment-induced absorption, to produce its singular, angle-independent brilliant blue colour. From the material design point of view, there are many elements to bring together to attain such complex optical effects: the reflecting elements must be on a subwavelength scale, need to be produced on a large scale, and must be sufficiently ordered to produce the desired colour and reflectivity. But it must also bear some disorder, on the subwavelength scale, in order to eliminate the directionality and sharp reflectance peaks associated with multilayered interference.

The colours in bird feathers are produced in two different ways, either from pigments or from light refraction caused by the structure of the feathers. In some cases, the combination of both effects may create more complex colour arrangements.[78] While structurally coloured barbules are normally composed of well-ordered melanin granules and rods,[79] the spongy keratin structures of weakly localised particles is responsible for structural colours in non-iridescent feathers[80] (see Fig. 2B and section 2.1).

Another intriguing phenomenon developed in nature is circular dichroism. The metallic-green colour of the beetles *Cetonia aurata* and *Chrysina gloriosa* is due to the chitin layers assembling into a highly uniform, helicoidal stack, which is optically analogous to a cholesteric liquid crystal. These circularly polarising multilayers reflect polarised light with a left-handed (anticlockwise) rotation. Some plants, such as in *Pollia Condensata*[46] and *Margaritaria nobilis*,[66] also use this strategy to produce iridescent colours. Analogous to beetles, their cellulose microfibrils form helicoidal stacks in the cell walls, which selectively reflect circularly polarised light of a specific wavelength (see Fig. 2C).

The iridescent colour of nacre, on the other hand, is the result of the biomineralisation process during which amorphous calcium carbonate ($CaCO_3$) and chitin sheets are sequentially deposited in the isolated space between the shell and the epithelium mantle cells. The crystallization of the $CaCO_3$ layers lead to lamellar stacks of calcium carbonate tablets separated by organic layers. The resulting ordered multilayer structure of crystalline $CaCO_3$ platelets causes the multilayer interference, displaying the characteristic pale green to pink iridescent colouration (see Fig. 1D).[81]

Natural mineralisation processes also engineer one of the most studied structurally-coloured systems in biomimicry. Precious opal is an amorphous form of silica ($SiO_2.nH_2O$) that contains water and that can be found in almost any kind of rock. Under suitable conditions, water percolates through the earth and drags silicates encountered in the soil. When this silicate-rich solution enters a cavity and the water evaporates, the silicates deposit as small spheres (with diametres ranging from 150 nm to 400 nm, in the case of rainbow-coloured opals). When the precipitated silica spheres are monodispersed in size, and stack in an ordered, close-packed fashion, they produce a play of colours by hugely coherent scattering in the visible light range (see Fig. 2D).[54,82]

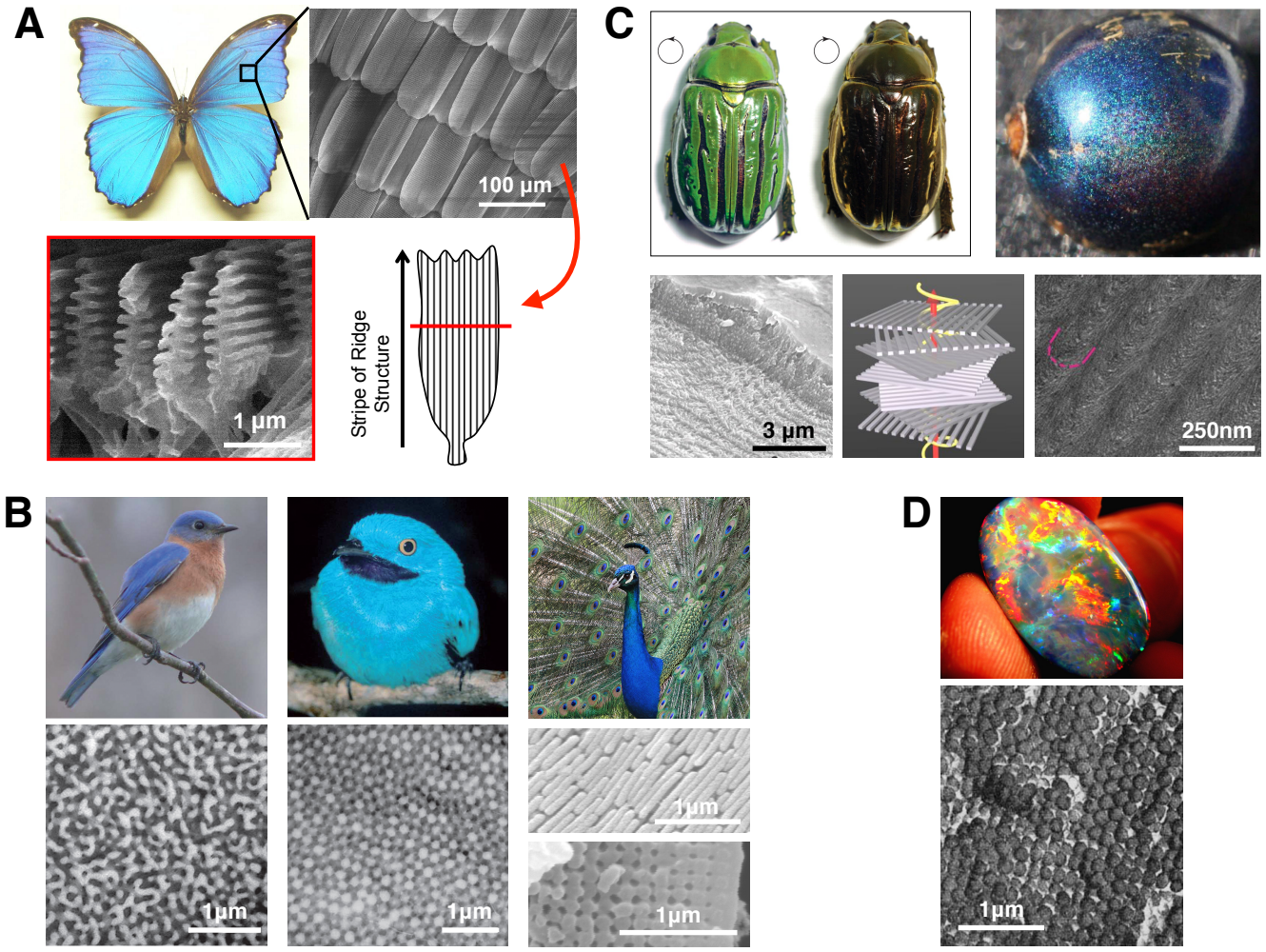

Fig. 2 Structural colours in nature that have attracted significant biomimicry efforts. (A) Typical *Morpho* butterfly (*Marpho didius*) and SEM images of the scale, each covered with ridges whose lateral profile has the typical "Christmas tree" shape (adapted with permission from Ref. 73, © 2006 Society of Photo Optical Instrumentation Engineers); the ridges are supported by a gyroid crystal structure that also produces structural colours. (B) Structural colours of the plumage in Eastern Bluebird (*Sialia sialis*, left) originate from quasi-order β-keratin tubular nanostructures, while in Plum-throated Cotinga (*Cotinga maynana*, centre), the structures are spheres (reproduced with permission from Ref. 74, © 2009 Royal Society of Chemistry); the peacock feathers (right) show 2D photonic crystals of melanin rods embedded in keratin (image of blue peacock *Pavo cristatus*: wikimedia commons; micrographs reproduced with permission from Ref. 52, © 2003 National Academy of Sciences, USA). (C) The Jeweled Beetles (*Chrysina gloriosa*) and the *Pollia condensata* fruit display circularly-polarized iridescence thanks to a structure of chitin (left micrograph) and cellulose (right micrograph) fibrils, respectively, similar to assemblies found in cholesteric liquid crystal shown in Fig. 7 (adapted with permission from Ref. 41, © 2009 American Association for the Advancement of Science, and from Ref. 46, © 2012 National Academy of Sciences, USA). (D) Natural opals display iridescent colours because of the crystal arrangement of silica spheres (image: wikimedia commons; electron micrograph reproduced with permission from Ref. 54, © 1964 Nature Publishing Group)

3 Biomimicry of natural structural colours

These unique characteristics of the structural colours developed in nature, such as iridescence or metallic appearance, cannot be obtained by mere chemical dyes or pigments. Therefore, in order to mimic the biological species, one needs to strategically design material composites with controlled variable nanostructures that can reproduce the biological structure itself.[83] Recent advances in controlling, and fine-tuning, the production and organisation of sub-wavelength structures have led to a burst of activities in the nano-photonics field. The fabrication methods can generally be classified into two groups:

- The *top-down* strategies involve using micro-fabrication tools to print computer-generated patterns using lithography techniques or multilayer deposition onto a larger piece of substrate. Although it is possible to produce a wide range of high quality photonic nanostructures with these technologies, the cost, efficiency and technical limitations (i.e. structures must be larger than 100 nm) of top-down approaches prevent their use in many applications with high throughput needs.

- On the other hand, the *bottom-up* approaches use the physicochemical interactions for the hierarchical organisation of nanostructures via the self-assembly of basic building blocks; these approaches are more cost- and time-effective, and widen the range of applications towards smaller accessible

length-scales.

3.1 Top-down strategies

3.1.1 Lithography.

In the last five decades, micro- and nano-lithography techniques have been developed to optimise the manufacturing of integrated circuits and microchips. Lithographic patterning can directly control the sub-micrometre structure on the reflecting surface of a dielectric material, and can thus be used to generate structural colours. Lithography techniques may be divided into two types, whether they use masks and templates, or not.[84]

The masked lithography transfers patterns from a mould or a mask template over a large substrate area simultaneously, thus enabling high-throughput fabrications. These lithography techniques include photolithography, holographic lithography,[85] nanoimprinting lithography,[86] and soft lithography.[87]

The second type of technique is maskless and fabricates arbitrary patterns by serial writing or etching. Examples of maskless lithography include electron beam lithography,[88] focused ion beam lithography, and scanning probe lithography. These techniques allow ultrahigh-resolution patterning of arbitrary shapes with a minimum feature size as small as a few nanometres. They are also often used to create the masks and templates employed by masked lithography.

We show in Fig. 3 the processes behind the lithographic techniques discussed here, and give below a few examples of their recent applications for the production of bio-inspired structural colours.

3.1.1.1 Photolithography. In photolithography, a photomask with a geometric pattern is transferred onto a light-sensitive chemical substrate (photoresist) by using visible or UV curing light (Fig. 3A). Lateral periodicities required to produce structural colours in the visible range are usually large enough to be patterned with photolithography.[89] Yet in many cases, the photolithography is coupled with self-assembled colloidal systems (see section 3.2.1) to further guide and control the shape and surface structure of the assembly.

Lee *et al.*[87], for example, successfully demonstrated the use of such coupled techniques to develop a 3D photonic crystal for reflection-mode display.[87] They first fabricated colloidal crystals that were embedded in a photoresist matrix on the surface of a substrate. The further photolithographic patterning of the embedded crystal enabled the creation of hybrid, micro-patterned structures. Selective removal of the colloids subsequently left a regular array of cavities, thus forming an inverse opal structure (see also Fig. 6C, described later) with a high index contrast between the air and the polymerised photoresist. Such structure produced a high reflectivity at the wavelengths falling within the photonic band-gap of the resulting crystal.

3.1.1.2 Interference & holographic lithography. Interference and holographic lithography is a versatile technique to fabricate both 2D and 3D periodic photonic structures in a scalable manner. In laser interference lithography, for example, the inhomogeneous distribution of energy, generated by the superposition of electromagnetic plane waves from two beams, is registered in a photoresist material coating a substrate (Fig. 3D).[85] There, 3D periodic patterns can be printed by adjusting the intensity, geometry, polarisation, and phase of the applied laser beams.[90]

Elaborating on this technique, Siddique *et al.*[91] were recently able to fabricate the complex, hierarchical "Christmas tree"-like morphology of the *Morpho* butterfly shown in Fig. 2A. They notably used a reflective coating between the glass and the photoresist to create an additional interference patterning perpendicular to the one obtained from straight dual-beam laser interference.[91] While the plain triangular morphology without lateral lamellae exhibited the usual grating effect at high angles, their *Morpho*-like structure reflected a blue colour by about 30%, over an extended range of reflection angle, between 0° and 40° (see Fig. 4A).

3.1.1.3 Nanoimprint lithography. The nanoimprint lithography (NIL) process creates patterned, 3D structures with feature sizes as small as 50 nm, by imprinting a stamp into a low viscosity resist via moulding (see Fig. 3C).[94] Since the process is based on direct mechanical deformation, the resolution constraints are only due to the structuring of the mould, as opposed to the usual limitations from light diffraction or beam scattering observed in conventional nanolithography methods. As long as the cast is stable, it is possible to produce many replicas from a single, prefabricated mould using this method.[86]

In an attempt to mimic the photonic nanostructures found on butterfly wings, Kustandi *et al.*[92] used NIL to produce tall and dense polycarbonate (PC) nanopillars. The surface adhesive force between those pillars and the intrinsically low modulus of the imprinted structures may cause an irregular collapse of the nanopillars in various directions. Therefore, in order to form an ordered structure, the researchers simultaneously applied a horizontal, shear-patterning force to the polymer during the mould release. This step allowed them to control the lateral collapse on the imprinted structures (see Fig. 4B). The periodic, unidirectional ridge arrangement made the structure work like a diffraction grating, while the multilayer seen from the top, due to the inclination of the pillars, gave the effects of interference and scattering. Consequently, their synthetic butterfly wings had angle-dependent optical properties, and showed both rainbow-type colour patterns and single colour patterns ranging from purple, blue, yellow, and red.[92]

NIL provides a simple, fast and cheap approach for the fabrication of nanofeatures with a high precision. Furthermore, it is possible to develop a high-throughput manufacturing process to imprint the patterns in a continuous manner, via roll-to-roll NIL.[95] While NIL exhibits a very promising future, it still has some issues in processing conditions, due notably to the mould's limited durability and the formation of defective structures when air is trapped in the gaps between the resist and mould cavities.

Based on NIL and soft lithography, other nanofabrication techniques, such as nano-casting lithography (NCL), have been developed with similar attributes, yet with some additional advantages. In their work, Saito *et al.*[73] produced a *Morpho*-type substrate by using NCL to produce a specific surface pattern. The created pattern was then coated with titanium oxide TiO_2 and

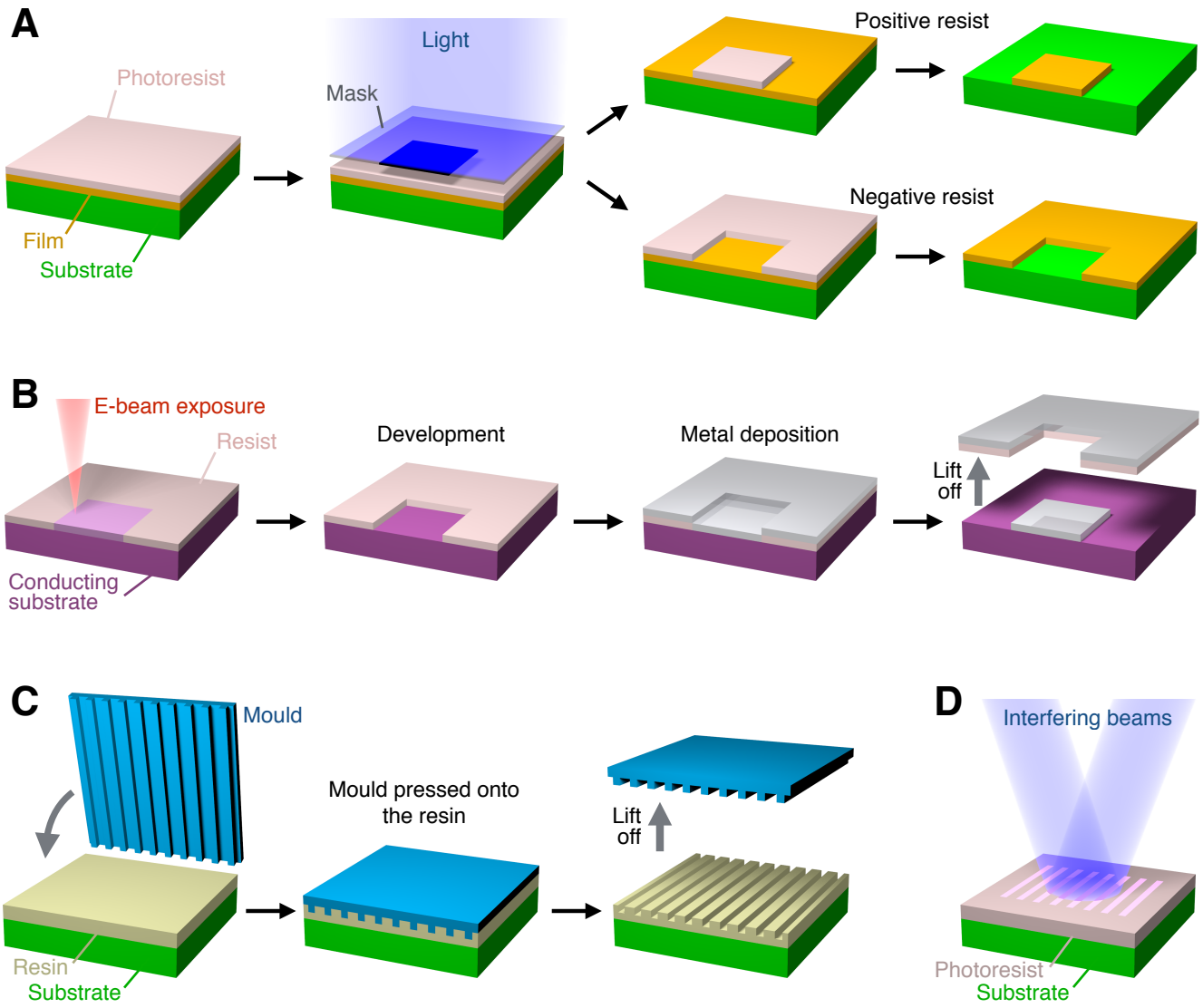

Fig. 3 Some top-down, micro- and nano-fabrication techniques used for the production of structurally coloured biomimetic materials. (A) In photolithography, a pattern is transferred from a mask to a photo-resist by a curing light; further chemical treatment develops the profiled layer. (B) Electron beam lithography serially registers a resist with a narrow, highly focussed e-beam. (C) Nanoimprint Lithography press-stamps a mould on a soft resin, which is then processed for its subsequent use. (D) Interference lithography does not use a mask, but exploits interference patterns to print a photoresist.

silicon oxide SiO_2 using successive electron-beam depositions, to form a multilayer with sufficient refractive index contrast. The optical properties of the resulting patterned multilayer showed many attributes similar to the *Morpho*-blue: hot and brilliant colouration over a wide angular range, high reflectance, slight change of the colour tone at a shallow observation angle, speckling, and one-dimensional anisotropy of the brilliance (Fig. 4D). Using such fabrication methods, one can further tune the colour by patterning the ridges, choosing the combination of inorganic materials, and controlling the multilayer thicknesses.[73]

3.1.1.4 Electron-beam lithography. Electron-beam lithography (EBL) is one of the most important techniques of maskless nanofabrication. It uses a highly focused electron-beam ("e-beam") to modify the solubility of an electron-sensitive resist material, thus allowing selective removal of either the exposed or non-exposed regions upon dissolution in a liquid developer (see Fig. 3B).[88]

In an another effort to reproduce the properties of butterfly wings colouration, Wong *et al.*[96] used EBL to design groove-based multi-grating structures that generate a specific blue structural colour observable over a wide range of reflection angles (16° to 90°). Exploiting the accuracy of EBL, they could change the geometry of the grooves on multiple hexagonal cells patterning the resist (poly(methyl-methacrylate), PMMA, in that case), each endorsing the effect of the grating size, orientation, density, and depth, on the colour formation and on the efficiency of light diffraction.

In a more recent study, Zhang and Chen[93] also mimicked the colouration of the *Morpho* butterfly wing scales by creating well-aligned and alternating lamellae structures of PMMA and lift-off-resist (LOR) using a novel process based on EBL. To create the air layers of the "Christmas tree"-like gratings in *Morpho*

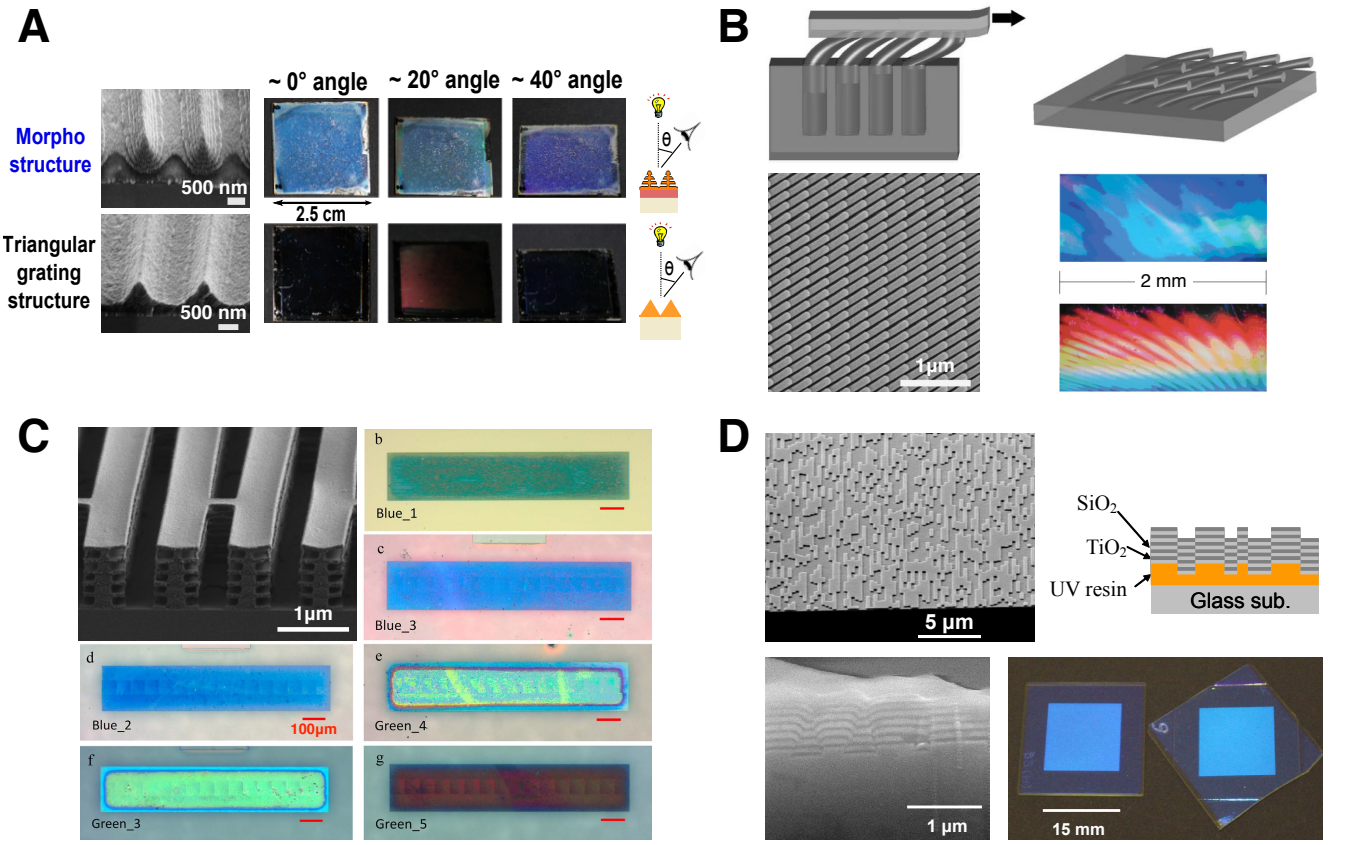

Fig. 4 Lithographic techniques employed to replicate *Morpho*-blue. (A) Laser interference lithography to produce a 3D surface patterning similar to *Morpho* butterflies' scales; the top is a blue-reflecting grating where each feature is laterally lamellar, the bottom is a simple grating with the same periodicity, but lacking colouration (reproduced with permission from Ref. 91, © 2015 Optical Society). (B) Nanoimprint lithography, combined with shear patterning, to fabricate uniformly collapsed pillars (adapted with permission from Ref. 92, © 2009 John Wiley & Sons). (C) Electron beam lithography can precisely sculpt lamellae structures similar to the ones found on the *Morpho* wing-scales (adapted from Ref. 93). (D) Nanoimprint or e-beam lithography is combined with layer-by-layer deposition to fabricate a multilayer-coated random grating (adapted with permission from Ref. 73, © 2006 Society of Photo Optical Instrumentation Engineers).

butterflies, the researchers selectively dissolved the LOR layers with a diluted alkali. Using this method, the colour reflection can be controlled by fine-tuning the layer thicknesses of both the PMMA and the LOR. Various colours, other than the *Morpho*-blue, can then be obtained (Fig. 4C).[93]

3.1.2 Layer-by-layer Deposition Techniques

Typically, multilayer photonic nanostructure films are fabricated using inorganic dielectric materials or inorganic nanoparticle/polymer composites. To obtain larger, variable stopband gaps, the layers may be designed with porous structures, and/or composed of stimuli-responsive polymer materials. Layer-by-layer (LbL) deposition methods, such as atomic layer deposition, electro-deposition, the Langmuir-Blodgett technique, and sputtering, lead to the formation of multilayers that are composed of periodic stacks with alternating high and low refractive indices. Although these methods usually result in well-controlled film growth, they often acquire high cost and suffer from scale limitations. Sol-gel-based depositions and spin-coating can offer more cost-effective routes to produce structural colours, but a high uniformity of deposition on curved substrates is then hard to achieve using these methods.

3.1.2.1 Liquid-based deposition. Silicon oxide (SiO_2, or silica) and titanium oxide (TiO_2, or titania) are widely used to fabricate biomimetic multilayered structures. They indeed have very different refractive indices ($n_{TiO_2} = 2.44$ and $n_{SiO_2} = 1.45$) and can easily be deposited from a liquid phase by spin- or dip-coating. Choi *et al.*[97] demonstrated the production of Bragg stacks out of porous layers by sequentially spin-casting meso-TiO_2 and meso-SiO_2 into a multilayer whose reflecting wavelengths' bandwidth exceeded 200 nm. In another work, Calvo *et al.*[98] demonstrated all-TiO_2 Bragg mirror production by changing the particle size in the sequential layers.[98] Fuertes *et al.*[99] assembled the same silica/titania nanoparticle pairs using a dipping process followed by humidity (24 hours) and thermal (> 48 hours) curing. They were able to achieve refractive index values of 1.35 and 1.82 for the resultant porous SiO_2 and TiO_2 nanoparticle stacks, respectively. Scharf *et al.*[100] constructed an optical system that combined Bragg reflectors and microlenses from poly(vinyl alcohol) (PVA) and poly(N-vinyl carbazole) (PVK). To do so, they used spin-coating of organic interference layers and soft replication of microlenses. Although their refractive index contrast between alternating layers was low, they nevertheless achieved a reflection

band centred at $\lambda = 570\,\text{nm}$.[100]

Kolle *et al.*[67] took the LbL technique one step further by combining spin-coating with multilayer-rolling in order to mimic the concentric layers found in the plant *Margaritaria nobilis*.[67] They fabricated a thin glass fibre, on which they rolled bilayers of two elastomeric polymers with sufficient refractive index contrast: polydimethylsiloxane (PDMS) with $n_{\text{PDMS}} = 1.41 \pm 0.02$ and polystyrene-polyisoprene triblock copolymer (PS-PI) with $n_{\text{PS-PI}} = 1.54 \pm 0.02$. Since the thickness of the layers controls the colour, the team could alter the appearance of these elastic rubber fibres upon the application of a thinning tensile stress. This example shows how structural colours can add functionalities to materials (see section 4), and such colour-morphing fibres could indeed create textile fibres for responsive athletic-wear, for example.

Mimicking the multi-layered structure of *Margaritaria nobilis* could be achieved using a simple spin coating of synthetic polymers. However in some cases, it is necessary to follow the steps taken in biogenic material synthesis in order to achieve the multifunctionality and optimised effects of optical and mechanical properties. This may indeed shed light on the fabrication of novel or low-cost materials. For this reason, Ullrich Steiner's group at the University of Cambridge (now at the Adolphe Merkle Institute) proposed a simple and robust approach to replicate the *natural* LbL process of nacre formation. The researchers created the multilayer by immersing a glass slide into poly(acrylic acid) (PAA) and poly(4-vinyl pyridine) (PVP) solutions sequentially. To introduce porosity into the PAA layers, they immersed the film in a basic solution which dissolved PAA, but also introduced surface functionalization to the substrate and the PVP layers, then stabilised by UV cross-linking. Mineral films were formed by ammonium carbonate diffusion technique, with a PAA solution that contained Ca^{2+} and Mg^{2+} ions to induce the formation of a modified calcite (cal_{org}) film. The film was further crystallised by exposure to high humidity. They repeated this procedure to create the organic/inorganic lamellar composite of the nacre structure. Through fine control over the layer periodicity, the researchers were finally able to reproduce the iridescence of the nacre.[81]

3.1.2.2 Vapour-based deposition. Chemical vapour deposition (CVD), on the other hand, allows high growth rates, as well as a profitable uniformity over large areas.[101] It is possible to deposit a great variety of inorganic structures through CVD, but the incorporation of organic materials instigates the creation of deformable and tunable photonic structures. Hence in their work, Karaman *et al.*[102] reported a Bragg reflector which consists of titania TiO_2, and of an organic material, poly(2-hydroxyethyl methacrylate) (pHEMA). This hybrid material can shift colour very rapidly and reversibly upon exposure to saturated water vapour, via the rapid swelling of the pHEMA layers.[102]

Another gas phase deposition technique, the atomic layer deposition (ALD), is used to produce thin films with a variety of materials. Based on sequential, self-limiting reactions, ALD offers exceptional conformality on high-aspect ratio structures, thickness control at the angstrom level, and tunable film composition.[103] Kolle *et al.*[104], for example, used a combination of techniques, including ALD, colloidal self-assembly, and sputtering, to fabricate photonic structures that mimic the colour-mixing effect found on the wings of the Indonesian butterfly *Papilio blumei* (see Fig. 5).[104]

3.1.2.3 Further examples of LbL-based biomimicry. The *Chrysochroa* genus of the metallic woodboring beetles exhibit glossy iridescent colours. The beetle cuticles are an example of a one-dimensional Bragg mirrors with a polarisation- and angle-dependent reflectance spectrum, typical for multilayer structure (see section 2.1). Furthermore, slight variations in layer thickness and/or refractive index cause variations in the colouration.[105] Inspired by the iridescent colour formation of *Chrysochroa* rajah beetle, Tzeng *et al.*[106] applied LbL deposition technique to polyethylenimine (PEI) and anionic vermiculite clay bilayers (high refractive index layer component), combined with cationic colloidal silica SiO_2 and anionic cellulose nanocrystals (CNCs, low refractive index layer) presented in section 3.2.1. The films produced had an even green color, resulting from the high consistency in layer thicknesses at the origin of the relatively narrow reflection band. The iridescence of the films was notably characterised by a blue shift of the reflected wavelength with increasing incidence angle.[106]

As explained in section 2.2, *Morpho* butterfly wings exhibit a complex optical response by combining several phenomena to produce a unique angle-independent brilliant blue colour. *Morpho* butterflies create these complex structures spontaneously, through self-assembly, without any directed construction. In order to address all the challenges of its biomimicry at the same time, Chung *et al.*[107] first produced a semi-ordered monolayer of silica nanospheres ($200 - 400\,\text{nm}$ in diameter) on a silicon wafer by spin-coating, and then further deposited blocks of TiO_2 and SiO_2 atop via sputtering.[107] By controlling the TiO_2 and SiO_2 layer thicknesses, they tuned the colour ranging from deep blue, through green, to coppery red. Notably, their deep-blue films are comparable to the *Morpho rhetenor*, with a peak reflectance of 55%, and its colour and brightness do not show significant changes across all viewing angles.[107]

3.1.3 Iterative size reduction

Iterative size reduction (ISR) is an alternative top-down technique to produce a flexible polymer fibre that consists of arrays of millions of ordered, indefinitely long, nanowires and nanotubes that can exhibit structural colours. Inspired by the composite-fibre drawing process from polymer reels, Mehmet Bayindir's group at Bilkent University demonstrated the fabrication of ordered arrays of nanowires by thermal ISR.[108,109]

The process comprises of a multi-step drawing of a fibre, starting with a macroscopic polymer rod. Each step starts with structures obtained from the previous one, resulting in geometrical size reduction and increment in wire number and length. At the end of the first thermal size reduction cycle, the cross-section of the fibres reduces from few millimetres to few micrometres. These fibres are then cut and arranged into a hexagonal lattice inside a protective jacket, that is vacuum consolidated and further redrawn for the second and third time. The authors showed the possibility of producing a variety of multi-material nanowire and nanotube structures, including nonlinear glass As_2Se_3 and ordered core-shell nanowires of As_2Se_3-PVDF

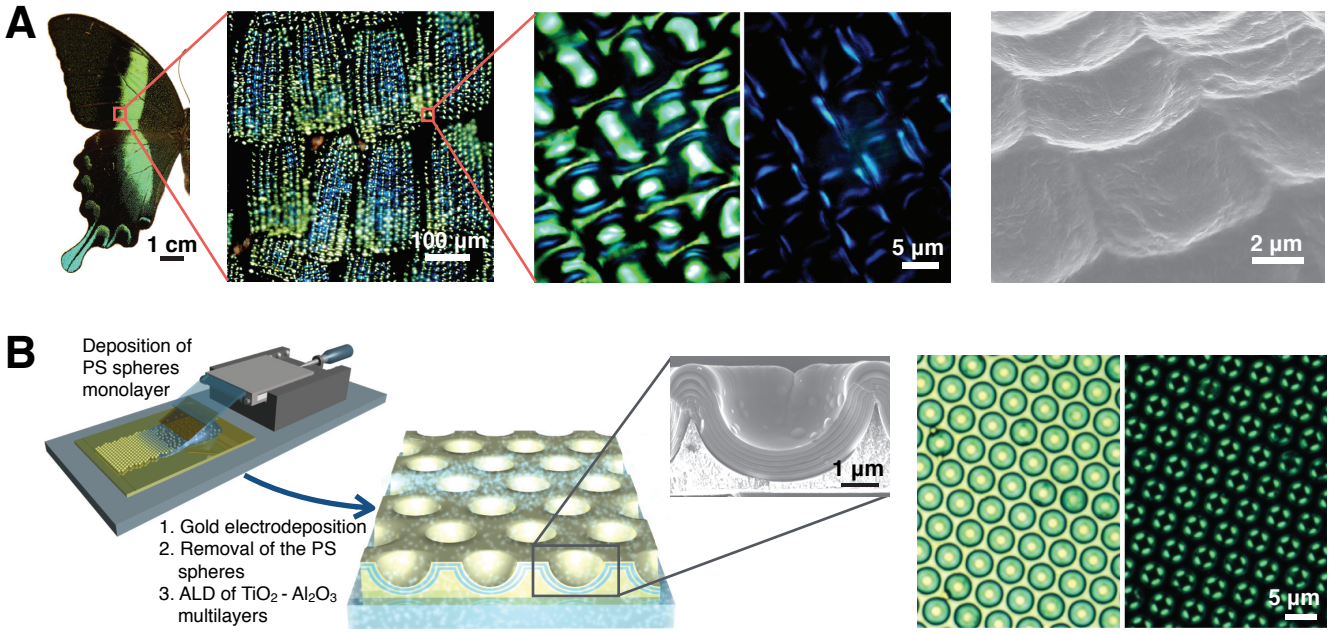

Fig. 5 *Papilio blumei* butterfly, biomimetic sample fabrication and optical mimicry. (A) The bright green wing of the *Papilio blumei* butterfly is shown at various magnification: a photograph of the wing; a zoom on the wing scales; further magnified optical micrographs of the wing scales observed without (left) and with (right) cross-porilazers; the rightmost image is an SEM of the *Papilio blumei* wing scale surface showing the concavities. (B) The deposition of polystyrene colloids on a substrate is followed by gold electro-deposition on the interstitial sites, removal of the PS monolayer and ALD deposition of Al_2O_3 and TiO_2 layers, to obtain concavities covered by a conformal multilayer stack of Al_2O_3-TiO_2 alternating layers, as shown on the SEM micrograph inset; the rightmost pair of images are light microscopy of the film that shows that the concavity edges are green, and the centres and interstitial regions are yellow (left), while only the green concavity edges are visible under crossed polarizers (right). Adapted with permission from Ref. 104, © 2010 Nature Publishing Group.

(polyvinylidene fluoride) in polyethersulfone (PES), which displayed structural colours. The colour formation, in this case, is explained by a combination of thin film interference from the core-shell nanowire structure, and Mie scattering from the core region (see section 2.1). The refractive index of each layer, as well as the core diametre, determine the scattered resonant modes in the vicinity of the nanowire, although thin film interference may dominate for appropriate shell thicknesses.

A more recent study from Bayindir's group reported the imitation of the peculiar 2D photonic structure in the neck feathers of mallard drakes. Using ISR technique, they produced a polymer composite fibre system, based on polycarbonate (PC) and PVDF which have low refractive index contrast ($n_{PC} = 1.58$ and $n_{PVDF} = 1.41$), but are thermally compatible for a successful processing with ISR.[110]

3.1.4 Combining top-down strategies

The control over features' shape and spacing, when patterning using these sophisticated lithography techniques, is particularly needed for the production of defect-free photonic structures with a well-defined and complete band-gap. By combining multiple lithography techniques together, or with other top-down fabrication processes such as deposition or chemical etching, a high-resolution 3D topography may be ultimately produced. And when further cycles of microfabrication steps are repeated successively several times, even more complex structures may be formed.

Hence, elaborating on their previous work[73] (described above in section 3.1.1.3) to replicate the delicate structural effects and optical response of *Moprho*-blue, Saito *et al.*[111] subsequently employed EBL and dry-etching to first fabricate a quasi-one-dimensional, patterned quartz structure, whose random discrete step-profiles have optimised widths and gaps sequence. They next used LbL to deposit a multilayer composed of alternating layers of TiO_2 and SiO_2 the patterned quartz substrate. The fabricated film shows the *Morpho*-blue, with some of its fundamental characteristics, such as hot brilliant blue in a wide angular range, and high reflectance. However, they were not able to reproduce the angular dispersion and wavelength dependence of the natural *Morpho*-blue.[111]

Nevertheless, and in spite of the advantage of fabricating nanostructures with precise morphology, a cost-effective manufacturing scheme to generate multicoloured structures over a large area is a challenge with top-down strategies, because of their usual requirement for a vacuum process.

3.2 Bottom-up strategies

3.2.1 Self-assembly

Self-assembly is the process by which a structural order at different scales is achieved without any direct external action.[112] One way to fabricate materials with structural colours is to create periodic nanostructures through self-assembly, using various building blocks, such as block copolymers, liquid crystals, and colloids. Nature, of course, uses this phenomenon in numerous cases to produce optimal colours and multifunctional materials. Therefore, it is important to understand the self-organised sys-

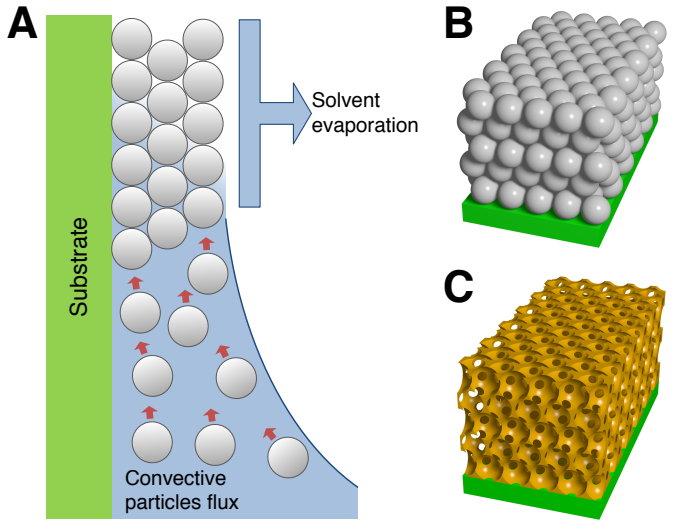

Fig. 6 (A) Self-assembly of multi-layer colloidal arrays through the vertical deposition technique. (B) Colloidal crystal in the opal structure. (C) The Inverse opal structure produced through infiltration of the opals, and subsequent selective removal of the colloidal spheres.

tems and processes found in nature, in order to replicate them "efficiently," from a technological point of view, with the goal to create defect-free, structurally coloured materials at large scales.

3.2.1.1 Colloidal self-assembly. Dielectric structures of colloidal systems, in the submicrometre length scale, can interact strongly with light. With specific designs, these can produce various and remarkable optical responses, which can be tuned further by altering the types and organisation of these structures. Self-assembled colloidal systems include colloidal crystals, composite and inverse opals, and photonic glasses. Owing to their unique optical properties and their applications as photonic crystals, they have now long been studied.[87] Colloidal self-assembly has significant advantages, and it notably offers the most facile and economical way to create 2D and 3D photonic crystals over large areas, and with a wide variety of possible shapes.[113] The optical properties of self-assembled, 3D colloidal beads (artificial opals) were first demonstrated by Astratov *et al.*[114] Since then, a great variety of materials, for both organic and inorganic microspheres, are used to produce biomimetic structural colouration through colloidal self-assembly. Among these, self-assembly of polymer opals, mainly consisting of polystyrene (PS) and PMMA monodisperse microspheres (Fig. 6B) in a face-centred cubic (fcc) arrangement, have been studied extensively.[112,115–119]

Several methods have been used to achieve long-range 3D arrangements through colloidal self-assembly. These include natural sedimentation of SiO_2 spheres followed by sintering,[120] electrophoresis of SiO_2 monodisperse nanospheres or SiO_2/TiO_2 core/shell particles,[121] or injection of PS beads into a confined environment.[122] Currently, the most commonly used method is the vertical, or convective, deposition method. This technique relies on capillary forces to organise colloid bases during the evaporation of the liquid (ethanol or water), which fabricates colloidal crystal multilayers (see Fig. 6).[123,124]

In order to tailor the photonic band-gap to a specific structural colour response, with added functionalities such as chemical sensing through a colour change, core-shell particles with various compositions were explored over the years. Hence, to control the position and the width of the wavelength band-gap, the core to shell compositions can be varied. Alternatively, it is possible to incorporate particles of different sizes into the interstices of core-shell particles crystals, in order to modify the final colour of the surface.[125] Moreover, one can also target the effect of refractive index contrast in the interparticle medium, as well as composition of the chemical core-interlayer-shell precursor particles, to effectively tune the colour.[126–128]

Natural materials are also often produced by self-assembly processes, and bear optimised structural order over multiple length scales to sustain maximum performance and multifunctionality. Most photonic crystals produced via colloidal self-assembly show brilliant structural colouring, due to the Bragg diffraction effect, which depends on the angle of observation (section 2.1). Therefore, a number of colloidal photonic crystals were recently developed with a macroscopic, spherical bead appearance.[129] Due to the spherical symmetry, the reflection spectra are unchanged upon rotating these photonic structure constructions, under illumination of the surface at a fixed incident angle of the light. This packaging may broaden the range of applications for photonic crystals. Tailoring the colloidal particles into a spherical shape that exhibits structural colour can be achieved with different arrangements within the macroscopic sphere: close-packed colloidal assembly,[130–132], non-close-packed colloidal assembly,[133,134] or inverse opals,[135] for example. Joanna Aizenberg's group at Harvard University also demonstrated colloidal crystallisation in an emulsion droplet producing micron-sized superstructures, which they called "photonic balls."[136] While the layered morphology of the colloidal spheres in the photonic balls gave rise to structural colouration, via Bragg diffraction, the natural curvature of the ball created a uniform, angle-independent colour formation. Such systems can have promising applications in optical devices such as diffraction gratings, colorimetric sensors or dispersible structural colour pigments.

Melanins are natural pigments found in several organisms, especially in the feathers, hair or skin of animals. They are thought to absorb UV radiation to protect the living organisms.[137] Birds use melanosomes to form organised structures for producing colours. Although such structures have already inspired the fabrication of photonic crystals, the use of melanins, or melanin-like materials, in structural colour biomimicry is a novel approach that was recently demonstrated by Xiao *et al.*[138] They prepared nanoparticles with an average diametre of 146 ± 15 nm and made of polydopamine (PDA), a type of synthetic melanin with refractive index $n_{PDA} = 1.7$. This particle size is within the diametre range of the rod-like melanosomes found in duck and peacock feathers, and thus replicates their structural features. They used a vertical evaporation-based self-assembly system to produce structurally coloured thin films. By tuning the thickness and/or concentration of the assembled nanoparticles, they were able to produce different colours, which all showed a good agreement with their theoretical model based on thin-film interference.[138]

The promise of colloidal self-assembly for the high-throughput

production of structural colours is indeed remarkable. However, the presence of unavoidable point -or extended- defects and cracks, accompanied by incomplete photonic band-gaps, still leaves colloidal self-assembly far from routine usage in photonics devices.[139] To overcome this barrier, many new strategies are being developed. For example, the use of selective chemical "glue", such as DNA or peptides, on particle surfaces has been proposed.[140] Further developments might enable the fabrication of better photonic devices based on colloidal particles. Moreover, recent progress in the synthesis of non-spherical particles is accelerating research into the colloidal assembly of new crystal phases.[141] One promising strategy, with a strong potential for producing new photonic properties, is to use directional interparticle interaction via chemical patterns on the colloids' surface, to create and design new types of colloidal lattices.

Colloidal self-assembly is a powerful platform for producing 3D patterned structures, with feature sizes ranging from a few nanometres to several microns. However, the variety of patterns that can be made through these bottom-up techniques is very limited, in comparison to top-down techniques. Therefore, recent years have seen several attempts to combine the top-down and bottom-up strategies for producing patterned colloidal photonic crystals. Hence, the production of uniform and crack-free structures, with high colour definition, has been demonstrated by using lithography techniques (section 3.1.1) on various inverse opal structures.[142–144] But the processes used in the fabrication of such structures are generally complex, time consuming and expensive.

Jeremy Baumberg's group at the University of Cambridge, on the other hand, developed a method to directly pattern colloidal crystals by using microimprint lithography, a facile and cost-effective technique. They notably assessed the effect of annealing the colloidal particles prior to the imprinting step, which affected the optical behaviour of the films. If the colloids are pre-annealed, microimprinting causes a compression of the imprinted region and changes the lattice separation normal to the surface. This effect results in dual-colour patterns. If the colloid crystals are not pre-annealed, microimprinting selectively peels the contacted region off the substrate, thus forming negative crystal patterns on the substrate. Such spatial control of colloidal assemblies and complex patterning may enable more advanced applications in, for example, sensing devices, pixelated arrays of structural colour units, or antifouling materials.[145]

3.2.1.2 Anisotropic particle self-assembly. Self-assembly of nanomaterials is a function of interparticle interactions (i.e. ionic charges, capillary forces, etc.), particle sizes, their distribution, and particle shapes. Various liquid-crystalline order structures, such as nematic, columnar, and smectic phases are observed for rod-like and plate-like particles at high volume fractions[146] (see Fig. 7). According to Onsager's theory, hard slender rods interacting with repulsive forces can exhibit orientational ordering at densities far below the closest packing. The thermodynamic stability of these ordered structures arises from a gain in translational entropy, which overrules the loss of orientational entropy associated with particle alignments.[147] A combination of a wide range of material properties, coupled by the self-assembly, could lead to numerous liquid crystalline phases and new materials with a wide variety of new applications.

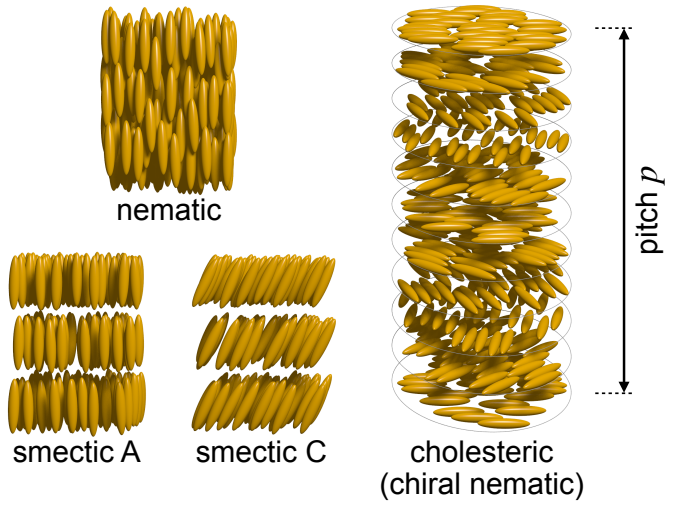

Fig. 7 Schematic illustration of a variety of liquid crystal mesophases, the nematic phase with only orientational order of the long axis of elongated molecules, the smectic phases (smectic A and smectic C) which exhibit additional one-dimensional positional order and chiral nematic (cholesteric) phase where the individual nematic layers stack together with a twist leading to helicoidal order with a pitch p, which refers to the distance over a full 360° twist.

As mentioned in section 2.2, nature also uses this strategy to produce iridescent colouration in plants.[46,66] The helicoidal-ordered stacks of cellulose are responsible for the bright colours in fruits and leaves of very different species of plants. Similar photonic structures can be artificially produced using the same constituent material, that is, cellulose nanocrystals (CNCs). Hence, the slow evaporation of a CNC suspension gives rise to their spontaneous assembly into a chiral nematic liquid crystalline phase that can be preserved in the dry state[148] (see Fig. 7).

Optically, chiral nematic phases have a number of interesting properties. First of all, they cause a significant optical rotation of the light, that is much stronger than that of the individual chiral components. Second, they strongly reflect light of a wavelength that is comparable to the length scale on which the nematic director makes one full turn, that is, the chiral nematic pitch p (Fig. 7). Interestingly, only circularly polarised light of the same chirality as the substrate is reflected, and the reflected light has the same polarisation (normal reflection on a metallic mirror, on the other hand, would cause the circular polarisation to invert). de Vries[36] explained these phenomena theoretically, and the reflected peak wavelength, is given by[36] the Bragg-Snell law, Eq. (1), where the half-pitch $p/2$ supplants the thickness d, and $\overline{n}$ is the average refractive index of the film ($\overline{n} = 1.55$ for CNCs[149]).

Several methods have been proposed to tune the chiral nematic pitch, and consequently the final colour formation in these cholesteric cellulose films.[150–152] Further investigations notably revealed that, within a single batch of cellulose crystallites, there are distinct domain formations of different periodicities, with different colour transitions, that can be correlated with the chiral

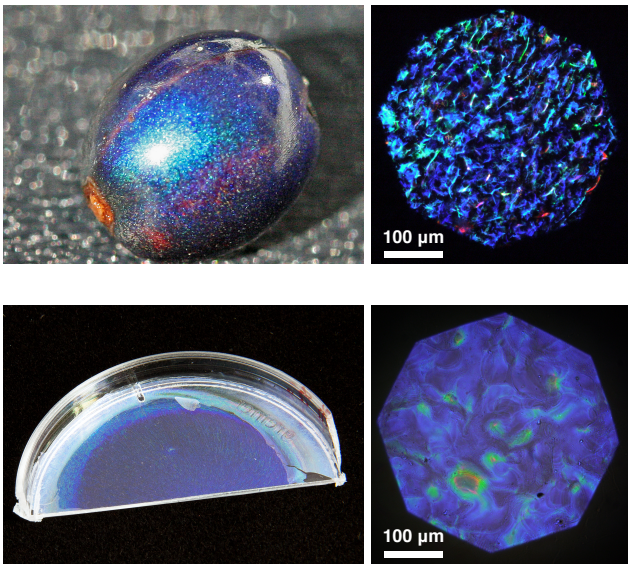

Fig. 8 (A) Photograph (left) of the *Pollia condensata* fruit and optical microscopy image (right) of its surface in cross polarisation configuration. (B) Photograph (left) of the chiral nematic cellulose nanocrystal (CNC) film and optical microscopy image (right) of the CNC film in cross polarisation configuration (reproduced from Ref. 154).

nematic pitch and layering (see Fig. 8).[153] Dumanli *et al.*[154] also demonstrated ways to control the CNCs self-assembly process, in order to produce a range of different colours selectively, yet starting from the same suspension.[154] In this work, they also developed an optical microscope setup to observe the film formation dynamics, while controlling the temperature and relative humidity, during self-assembly, in an environmental chamber. Their findings revealed that the CNCs self-assembly starts from a completely random organisation and, with gel formation, the small domains of chiral nematic stacks progressively appear. Just before the complete drying, they observed that the films formed display colours in the red, and subsequently shifts colour due to evaporation of water.

Chitin nanocrystals are also found to form chiral nematic phases in concentrated suspensions, in which the chiral nematic phase can be preserved upon drying of the film. However the film does not show structural colour formation in the visible range, and the optical activity for such chiral nematic systems was indeed observed in the infrared region.[155]

3.2.1.3 Block copolymer self-assembly. Nanostructures based on block copolymer (BCP) self-assembly have been employed in the fabrication of a large number of photonic crystal structures, from one to three dimensions. BCPs are macromolecules that consist of different monomer sequences organised into continuous blocks. Typical BCPs are linear and contain two or three major monomer blocks, say A, B and C, organised such as AB, ABA or ABC.[156]

Chemical incompatibility between the constituent blocks results in phase separation between the two blocks, whilst the covalent linkage between the blocks restricts the phase separation to the length scale of the polymer molecules (typically, a few tens of nanometres). The spontaneous aggregation of the individual blocks towards an equilibrium condition yields well-defined structures, based on non-covalent interactions. There are four classes of morphologies arising from such phase separation: lamellae (L), hexagonally packed cylinders (H), body-centred spheres (Q^{229})and the double-gyroid phase (Q^{230}),[157] as shown in Fig. 9. The main parameters that determine the phase morphology of an AB diblock copolymer are the volume fractions of the blocks f, and the degree of segregation, χN (see Fig. 9B).

It is evident that multi-directional photonic band-gaps exist in these structures, and the reflected wavelength λ_m is proportional to the material periodicity d, and can be again approximately expressed using the Bragg-Snell law, Eq. (1), for each order of diffraction m. As before, $\bar{n}$ is the average refractive index of the reflecting elements. Most polymers have a refractive index around 1.5. Thus, to obtain a photonic band-gap of visible wavelengths, the periodic spatial modulation of the refractive index has to be on the order of 120 nm or larger. The typical unit cell dimensions for self-assembled BCP morphologies are on the order of $5-100$ nm, which makes them unsuitable for visible photonic band-gaps.[159] Therefore, the main challenge with BCP-based photonic structures is to produce larger structures with periodicity comparable to the wavelength of visible light. Increasing the unit cell size in two and three dimensionally continuous morphologies is arduous. Nevertheless, the use of the gyroid phase for optical illusions can actually be seen in nature; for example *Callophrys rubi* butterfly wing scales exhibit a highly ordered, porous, three-dimensional single gyroid structure which extends throughout the scale, beneath the ribs and the cross-ribs. Due to the chiral orientation of the gyroid phase, the butterfly indeed displays circular dichroism.[160]

There are numerous efforts put into the development of BCP-based photonic crystals that reflect light, as well as change colour in the visible region. A photonic response in the visible range requires reliable phase separation, and a high degree of long-range order in, usually, very high molecular weight BCPs.[161] However, high molecular weight (that is, greater than $1\,\mathrm{Mg\,mol^{-1}}$) materials are extremely viscous in the melt, and do not easily self-assemble into well-ordered structures due to their strongly-entangled configurations. Yet, self-assembled BCP photonic crystals are highly responsive to different kinds of external stimuli such as solvent, temperature, or compressive mechanical strain.

One interesting example of solvent stimuli was recently demonstrated by Chiang *et al.*[162]. They fabricated a responsive BCP photonic crystal system based on high molecular weight polystyrene-polyisoprene (PS-PI) block copolymers, with a lamellar morphology in toluene. When the polymers were in a relatively low-concentration regime, that is, at a concentration ϕ_p only slightly higher than the order-disorder transition concentration, $\phi_{ODC} \lesssim \phi_p$, a red-shift reflectivity band could be seen. This was due to the thermodynamically controlled swelling of BCP's long period by the intensified BCP's segregation strength. By contrast, in the high-concentration regime $\phi_{ODC} \ll \phi_p \leq 1$, a blue-shift reflectivity band was seen, and attributed to the kinetically controlled deswelling of the BCP's long period by the collapse of the block chains.[162] The mixtures of selective and

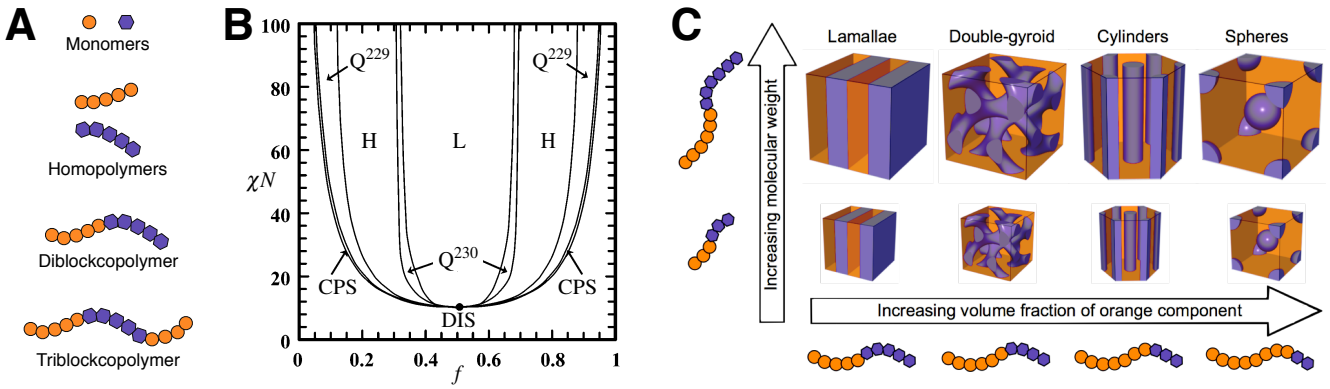

Fig. 9 (A) Block copolymer system building blocks. (B) Theoretical phase diagram for a linear diblock copolymer (adapted with permission from Ref. 157, © 2006 American Chemical Society) in the degree of segregation χN vs block's volume fraction f space; the various equilibrium morphologies are lamellae (L), hexagonally packed cylinders (H), body-centred spheres (Q^{229}), the double-gyroid phase (Q^{230}) and the close-packed spheres (CPS); otherwise the system is disordered (DIS). (C) Block copolymers and self-assembled equilibrium morphologies (adapted with permission from Ref. 158, © 2013 Springer).

neutral solvents for diblock BCPs are quite successful in fabricating structures with finely-tuned photonic properties. Matsushita and Okamoto [163] demonstrated an example of the effect of the solvent, which can selectively swell one or both of the blocks of a symmetric polystyrene-*block*-polyisoprene (PS-*b*-PI) diblock copolymer system. [163]

Alternatively, by blending the BCP system with nonvolatile solvents or homopolymers, the periodicity of the structures can be tuned over length scales that enable them to interact with visible light. [164] For example, Urbas *et al.* [165] demonstrated a mix of diblock PS-*b*-PI copolymer with its constitutive homopolymers, which formed lamellar structures with reflection peaks in the $330-620$ nm range, depending on the blend composition. [165] A reversible switching of an optical band-gap is also possible, as demonstrated by Valkama *et al.* [166], using polystyrene-*block*-poly(4-vinylpyridinium methanesulfonate) and 3-*n*-pentadecylphenol supramolecular diblock systems (PS-*b*-$P4VP(MSA)_{1.0}PDP_{1.5}$). The prepared films had long-ordered periodicity, around 160 nm, and reflected green colour. As the system was heated above 125°C, the film lost its colour, due to the disruption of hydrogen bonding. This indeed induced a very strong decrease in the long period of the lamellar structure, within a narrow temperature range, because of more compact polymer coiling. [166]

The interaction of the polymer blocks with its own chemical environment and applied fields can also alter the total volume fractions of the lamellae. An example of a pronounced manifestation of this effect was shown by Hwang *et al.* [167] in an electrochemical cell which consists of a BCP system of alternating polystyrene (PS) and swellable poly(2-vinylpyridine) (P2VP) gel layers, with pH-dependent photonic band-gaps. The optical response of these photonic gels was tuned, and further optimised, by controlling the ion-pairing affinity between the protonated pyridine groups and their counter anions. [167] The photonic band-gap of the PS-*b*-P2VP can be tuned by different strategies, such as UV-exposure [168] or by adding reactive monomers to the film. [169] It is also possible to process the PS-*b*-P2VP in poly-vinyl alcohol to form ellipsoidal nanoparticles. This eliminates the angle-dependent view arising from one dimensional construction in the films. [170] More recently, Park *et al.* [171] reported an electrically switchable, free standing film from a self-assembled poly(styrene-*block*-quaternized 2-vinylpyridine) (PS-*b*-QP2VP) copolymer as well. [171]

Two recent reviews on photonic structures using BCP's self-assembly rationalise the prospect of these: while it is still a very promising approach for the scalable production of photonic crystals and structurally coloured, functional materials inspired by nature, the working examples are still mostly limited to one-dimensional structures. [159,172] On the other hand, the production of BCP's 3D-nanostructured photonic materials for the visible range remains an important challenge.

3.2.2 Biomimetic templates

Templating is a common technique in materials science that permits control of the morphology of materials at different scales. By using the template strategy, it is even possible to achieve material properties that are different than the host (template) material itself. The infiltration of the secondary components is usually done via the deposition of the other compounds (guests) onto the template, by means of different techniques such as sol-gel processes, [173–176] ALD [177] and CVD [178] (see section 3.1.2.2). Replicas are created after the sacrificial scaffold is removed from the system without disrupting the morphology, via heat treatment, chemical treatment or subsequent growth.

While transparent polymers are quite successful at mimicking the natural structural colour formation phenomenon through self-assembly, added functionalities often rely on high refractive index contrast or surface plasmon effects that are not yet accessible with these soft materials. A great advantage of the templating method is that it is very general with regard to the types of materials that can be prepared. Hence, it is possible to extend the material properties of soft materials with added compositions, such as conductive polymers, metals, semiconductors or graphitizable carbons. [179]

One can usually reproduce the exact intricate nanostructures seen in nature, by using the actual biological structures as templates, through gas- and solution-based deposition techniques

(see also section 3.1.2). Direct replica, or inverse of the structures, can be generated after the removal of templates. For example, Huang *et al.* [177] directly deposited Alumina (Al_2O_3) onto the scales of *Morpho Peleides* using ALD. [177] When the biological template was removed, they obtained an inverted Al_2O_3 shell structure, which replicated the morphology of the wing-scale structure, as seen in Fig. 10. Furthermore, some of the optical properties, such as the photonic band-gap, were also inherited by the alumina replica. The reflection spectral analysis of the replicas indicated a shift in the reflection peak to longer wavelength than the typical purple-blue reflection of the *Morpho*, because of the change of periodicity and refraction index. The researchers were also able to tune the shift in the reflection wavelength by changing the thickness of the Al_2O_3 layer ($10-50$ nm, see Fig. 10A).

Instead of removing the biological template, it is also possible to deposit the inorganic material and leave the biological template as the organic scaffold, in order to retain the mechanical properties. Hence, Liu *et al.* [180] produced such organic-inorganic hybrid material by coating the *Morpho menelaus* wing scales with Al_2O_3 in an ALD chamber. Their work on optical properties of both natural and organic-inorganic hybrids reveals that the iridescence and diffraction characters of the fabricated hybrid structures are homologous to the untreated specimen. Besides, both the uncoated and coated wing-scales showed hydrophobic characters with similar wetting contact angles of 114° and 119.5°, respectively. [180,181] In a similar study, Gaillot *et al.* [182] tried to work with amorphous TiO_2 deposited onto (route I: deposition on the outer surfaces) and into (route II: deposition on both outer surfaces and inner surface through pores and cracks) the scales of *Papilio blumei* butterfly (see Fig. 5A), by using low temperature ALD. [182] In this work, the researchers demonstrated that the TiO_2 layers form a unique, hybrid organic-inorganic Fabry-Pérot resonator. It was also possible to control the spectral intensity and colouration, by controlling the deposited TiO_2 thickness.

The solution-based deposition methods involve the chemical treatment of the wing scales to remove the pigments, dipping the wing scales in the sol-gel precursor, the heat treatment process for crystallisation of the metal oxide, and finally the removal of the biological template. Although the possible wet chemistry treatment on *Morpho* butterflies was demonstrated for ZnO and TiO_2 in rutile form, [174,183] these replicas did not display the optical properties of the template itself. This was due to disruptions of the order and periodicity in the metal oxide structure. Chen *et al.* [184], on the other hand, managed to deposit ZrO_2 onto *Euploea mulciber* wing scales using a modified sequential dip-coating sol-gel method. They started with bleached wing scales, to remove all organic species. Upon removal of the biological template, the inorganic replicas showed angle-dependent iridescent colouration due to the high refractive index of ZrO_2 ($n_{ZrO_2} = 2.16$). Their work indicated that the ZrO_2 precursor was able to deposit onto the intricate structure of the butterfly wing scales, without disrupting its morphology. [184]

Biological templates are important to both study and understand the hierarchy and the evolutionary pathways employed to create colour through material structure. But the biomimetic structures themselves can also be used as templates in a more

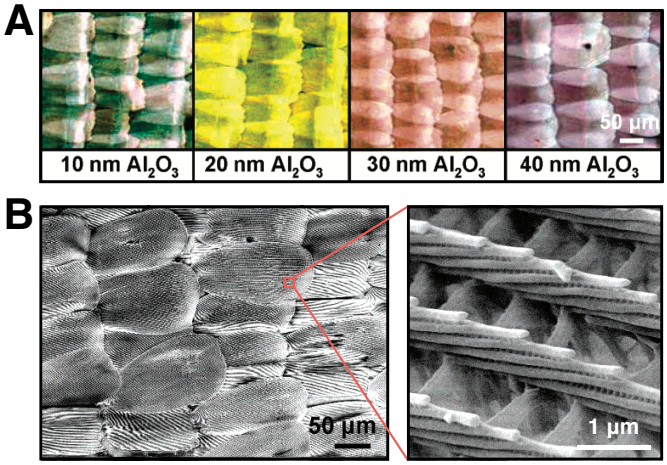

Fig. 10 Images of the Al_2O_3 replicas of the *Morpho peleides* butterfly wing scales. (A) The optical microscope images of the alumina coated butterfly wing scales, with different thicknesses of Al_2O_3 deposition. (B) SEM image of the alumina replicas of the butterfly wing scales after the butterfly template was completely removed (left); a higher magnification SEM image of an alumina replicated scale shows that the replica exhibits the same fine structures (right). Adapted with permission from Ref. 177, © 2006 American Chemical Society.

scalable manner. By using the self-assembled systems as a template, for example, the ability to control the periodicity and structure at nanoscales has a tremendous potential to develop many novel functional materials. The self-assembled systems can be used as direct templates, by infiltrating the second material once the self-assembly process is finished, or they can be used as structure-directing agents that allow the insertion of the second material to follow the specific morphology.

3.2.2.1 Direct Templating and Inverse Opals. The development of synthetic opals as 3D photonic crystals naturally pushed the researchers to fabricated these systems with material composites in order to boost their potential. This was done by either increasing their dielectric contrast, or most notably, by incorporating active elements (chiefly emitters) to modify their spontaneous emission for low-threshold laser sources. This pursuit has favoured the enormous development observed in the last few years, regarding experimental realisations of opal-composites with a large variety of materials. These efforts have undoubtly pushed and enriched the state of the art in materials science. [185]

The general concept for producing inverse opals is simple. First, one has to form the opal itself, then fill the interstitial spaces with a liquid precursor material (polymer solution, sol-gel precursor or a homogeneous dispersion of nanoparticles), and finally, once the precursor has solidified within the template, the opal structure is removed through chemical dissolving, radiation or heat treatment. Inverse opals offer a great palette for the production of tunable structural colour, and have been the subject of several review papers. [113,186] Many examples of chemical infiltration in the opal structure, via inorganic sol-gel precursors, including TiO_2, SiO_2 and Al_2O_3, were successfully demonstrated. [187–190] The inverse opals not only show promising applications in thin-film configuration, but can also be processed in a powder form

to produce additive structural colour pigments (see Fig. 11A), as demonstrated by Josephson *et al.* [191] Gas phase infiltration methods, such as CVD [192,193] or ALD [194,195] (see section 3.1.2.2), have also extended the possibility of production of inorganic inverse opal materials in various configurations. These techniques indeed allow very conformal deposition around the spherical units, with controllable thickness, which is essential to control both the homogeneity and the optical properties.

Silica opals, on the other hand, are very useful for the fabrication of inverse opal structures, where the guest materials require further thermal and chemical treatment. Silica is indeed thermally stable at elevated temperatures (circ. 700°C), and chemically inert in the presence of most solvents. It is also possible to infiltrate the silica opal structure with polymers to form structurally coloured, free-standing films with long-range order. [196] Even more intriguing systems, where the biological materials are themselves constructed in a photonic organisation by the template infiltration method, may also be explored. Hence, in a recent communication, Kim *et al.* [197] reported the use of silk in an inverse opal structure. Starting from PMMA opal templates, they infiltrated fibroin solutions extracted from *Bombyx mori* silkworm cocoons, and allowed the silk to solidify into an amorphous, free-standing silk-PMMA film. The PMMA templates were then removed by dissolution in acetone, which led to the formation of iridescent silk films. [197]

The combination of templates, materials composition and engineered photonic nanostructures are endless, thus offering vast possibilities for various applications (see section 4). The further incorporation of functional dopants, photoactive or photochemical compounds, or nonlinear optical elements, are also routes for even more sophisticated properties.

3.2.2.2 Co-assembly. As mentioned in section 3.2.1.1, the use of self-assembly processes to form large-area colloidal crystal films typically results in the formation of cracks, domain boundaries, colloid vacancies, and other defects. The subsequent solution-based infiltration of such templates causes additional cracking of these mechanically fragile templates. In order to avoid further deformations in the opal (or inverse opal) structures, and increase the strength of self-assembled templates, partial sintering, [198] deposition onto topologically patterned substrates, or changing the evaporative deposition conditions were suggested. [199] However, excessive infiltration and deposition may still result in overlayer formation, whereas incomplete, or non-conformal, deposition often leads to structural collapses during the removal of the template. Therefore Aizenberg's group recently made significant efforts to produce crack-free and uniform large area inverse opal films. In their work, they discovered that letting the colloids and a silicate sol-gel precursor co-assemble in a single step, rather than the classical sequential replication, actually generates highly ordered, crack-free, multilayered inverse opal films on the scale of centimetres. They also reveal the mechanism to achieve such long-range order. Co-assembly indeed eliminates cracking and inhomogeneity, which are associated with liquid infiltration into a preassembled opal. Furthermore, this method takes advantage of the interplay between the template and the matrix's assembly, leading to the further correction of incipient defects. [200]

At the other end of the scope, chiral nematic self-assembled systems can also be used as structure-directing agents for self-assembly. Interestingly, for such systems, infiltration with a sol-gel precursor leads to the production of mesoporous metal oxides, without replicating the chiral nematic CNC structure. [201,202] Once the CNC self-assembly takes place, the strong interaction between nanocrystals leads to the formations of a compact structure, which does not allow the guest molecules (or particles) to infiltrate. Therefore, Mark MacLachlan's group at the University of British Columbia developed a method where the CNCs self-assemble in the presence of a silicate sol-gel precursor, tetramethylene orthosilicate (TMOS). The researchers were able to demonstrate the first example of using CNCs as a structure directing agent for the production of free standing SiO_2 chiral nematic films with structural colour. [175] The helical pitch of the silica films could be tuned across the entire visible spectrum, and into the near-infrared, by adjusting the proportion of the silica precursor TMOS to CNCs. The same approach was extended to other sol-gel precursors, such as organosilicates, $(RO)_3Si\text{-}R'\text{-}Si(OR)_3$ where R' = aliphatic/aryl, to produce periodic mesoporous organosilicas. [203] The same team was also able to transfer the chiral nematic structure to water soluble resins. [204] Per further functionalisation of the surface charges of the CNC, they were further able to disperse the CNCs in different solvent systems to fabricate chiral nematic composite films of CNCs with PMMA and PS. [205] These systems all had chiral nematic pitch in the visible region.

Chemical infiltration into the structurally coloured media entails the transport of chemicals to the reaction site, which takes place in pores of only few hundreds of nanometres (sometimes, even less). Therefore, access to the reaction sites is often limited. Furthermore, when the chemical precursors initiate material growth on the walls of the pores, access to these sites diminishes as the reaction simultaneously proceeds. This effect puts a limit on what thicknesses can be grown. Hence, co-assembly, potentially solving these problems, seems to be a very promising method for the template approach, and more generally, for the synthesis of diverse new porous materials with attractive optical properties.

4 Applications

As already explained, colours play a vital role, both in the plant and the animal kingdoms, by providing ways to communicate, to entice or to camouflage. [207] The interaction of light with micro- and nano-structures can produce various optical phenomena, some of which result in structural colouration without using pigments. The pigments rely on the absorption of certain wavelengths of light. As a result, other wavelengths are reflected or scattered, which causes the observer to see the corresponding colours. When chemical pigments absorb light, they trigger a series of chemical interactions within the material, which may cause them to fade over time. Structural colours, on the other hand, potentially endure for much longer time scales. Furthermore, from an environmental standpoint, biomimetic structural colouration has an ecological merit since they are not produced

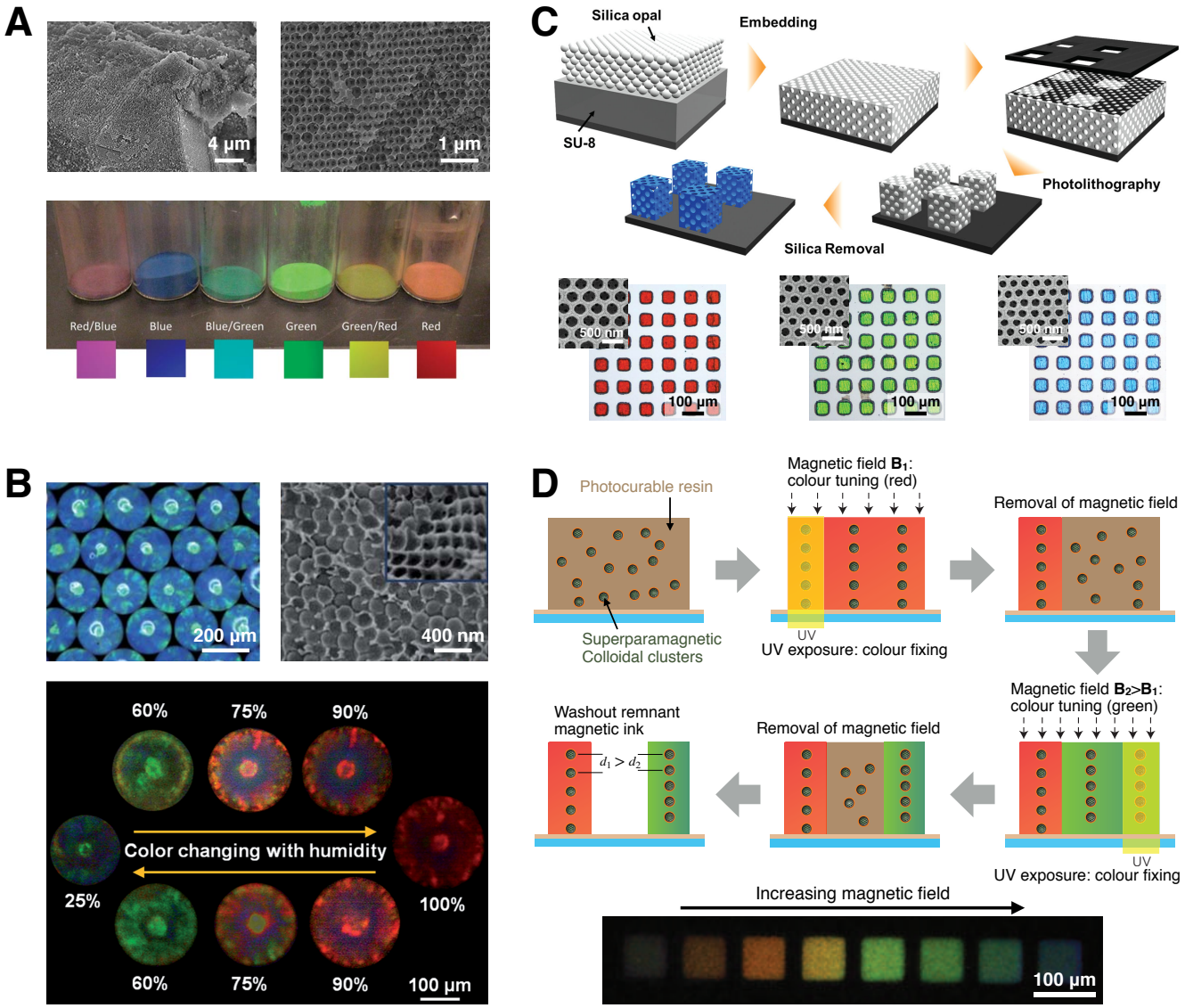

Fig. 11 Examples of recent applications of bio-inspired structural colours (A) SEM images of inverse opal SiO_2 powders at two magnifications (top), and photography of the mixed primary colour pigments (adapted with permission from Ref. 191, © 2014 John Wiley & Sons). (B) Optical microscope and SEM images of PS colloids immobilised in polyacrylamide hydrogel (top), forming the photonic supraballs; reversible colour changes of the supraballs with varying relative humidity (adapted with permission from Ref. 131, © 2013 Royal Society of Chemistry). (C) Illustration of SU-8 photoresist inverse opal fabrication, and optical microscopy images (corresponding SEM in insets) of the pixelated inverse opals prepared to reflect a single colour: red, green or blue (adapted with permission from Ref. 142, © 2014 John Wiley & Sons). (D) Illustration of the patterning of the "magnetic ink" made of superparamagnetic colloidal nanocrystal clusters embedded in photocurable resin; the diffraction wavelength (d_1 and d_2) is tuned by varying the strength of the magnetic field. The spatially patterned UV-light polymerises the resin and fixes the position of ordered colloidal clusters; the bottom image are optical micrographs of the multicoloured structural colour generated by gradually increasing magnetic fields in reflection mode (adapted with permission from Ref. 206, © 2009 Nature Publishing Group).

through chemical processes. Understanding the mechanism behind structurally coloured systems in nature is therefore of high importance. Not only may it shed some light on evolutionary processes, but it could also offer a route to yet unknown technological prowess. Nature uses cost effective materials, and simple, finely selected processes, in order to develop multifunctional materials. Therefore, mastering nature's concepts for material design opens new doors for today's advanced technologies.

4.1 Responsive and tunable structural colours

One of the most studied areas for structurally-coloured materials is their response to surrounding environmental stimuli producing a change in colour. The colour of such stimuli-responsive photonic band-gap materials are changeable by varying either the distance of two neighbouring lattice planes, or the refractive index contrast between two media. Therefore various responsive structural coloured materials have a great potential for the development of materials in many different industries, from advanced textiles to optical sensing devices and actuation systems.

Mechanochromic solid sheets, or structural colours in hydrogel form, have been widely explored as the basis of smart and functional fabrics. Various methods have been proposed for the fabrication of solid mechanochromic sheets, including crosslinking of mono-dispersed core-shell microspheres consisting of a rigid core and a soft, elastomeric shell. These offer rapid, reversible and repeatable colour transitions upon the application of a stress and its removal. Further methods include the infiltration of an elastomer into assembled hard microspheres, to form non-close-packed colloidal, inverse opal structures.[208–213] It is also possible to produce photonic hydrogels by fixing monodispersed magnetic nanoparticles i.e. Fe_3O_4 within the hydrogels, under a magnetic field, and by further *in situ* photopolymerization in a cross-linked acrylamide (AM) matrix.[214]

It is also possible to process similar biomimetic photonic structures in a fibre form, in order to produce flexible and "smart" photonic textiles with colors that are tunable over the entire visible spectrum. These can then also act as optical sensors for both strain and pressure. Hence, as mentioned in section 3.1.2.1, Kolle *et al.*[67] produced a multilayered fibre that is spun around a glass filament, and that essentially forms a planar Bragg stack. Upon removal of the glass core, the resulting flexible fibre showed sensitive colour changes against an applied strain. Such biomimetic fibres could potentially find applications in mechanically tunable light guides or optical strain sensing.[67]

Similarly, Sun *et al.*[215] demonstrated the fabrication of mechanochromic fibres based on aligned carbon-nanotube (CNT) sheets. These were bound to an elastic PDMS fiber, with polymer microspheres deposited on the CNT layer electrophoretically, and followed by further embedding in PDMS to fix the microspheres.[215] An alternative method for the production of structurally coloured strain-responsive fibres was suggested by Shang *et al.*[216], again based on fixing magnetic nanoparticles (Fe_3O_4) in a polyacrylamide glycol gel matrix. Upon the application of an external magnetic field, the randomly dispersed spherical particles are embedded in the matrix as 1D chain-like structure. The distance between each sphere in the matrix can be reversibly changed by elastic deformations of the matrix, which produce a visible colour change.[216] Zhang *et al.*[217] recently developed a different strategy to prepare mechanochromic fibres. They coated, continuously, commercially available black spandex fibres with microspheres made with a hard, PS/PMMA core and a soft PEA (poly(ethyl acrylate)) shell. They demonstrated that the microspheres self-assemble into a photonic crystal structure with brilliant structural colours that cover the visible light region. They could also control the colours of these fibres by varying the diameters of the core-shell microspheres.[217]

Novel materials, made via the rapid formation of ordered arrays through a change in magnetic or electric fields, and with widely, rapidly, and reversibly tunable structural colours are desirable for various chromatic applications: colour display, security, camouflage, or information storage, for example. The key to tune the self-assembly, and hence the colour variations of such systems in response to a magnetic field, lies with the formation of a dynamic balance between magnetic dipole-dipole interaction and long-range electrostatic repulsive interactions. This process, however, requires the use of specialised magnetic colloidal particles. Different magnetic colloidal systems, based on superparamagnetic Fe_3O_4 nanoparticles or nanoellipsoids made of a metallic Fe core inside a SiO_2 shell, were shown to align under magnetic fields spontaneously. These systems are very promising to produce magnetically responsive photonic systems as a new platform for chromatic applications.[218–220] Electric fields, on the other hand, can also assemble colloidal particles into ordered structures that dissipate into a disordered phase on removal of the electric field.[221] It is indeed common to examine the reorganisation of colloidal crystals under an electric field in a liquid medium.[222,223] Further to these, Baumberg's team devised a method to fix the electrically-induced particle chains in a polymer matrix permanently, which can potentially be the basis of a new scanning printing process. Since it is difficult to replicate the patterning process and the structural colours, such systems can find a market value where iridescent, non-fading structural colours are favourable, such as printing on banknotes, passports, and certificates.[224]

The colorimetric response of structurally coloured systems to temperature changes,[225–227] as well as the colour changes against chemical interactions in the gas phase or through liquid solvent interactions (such as solvent vapour infiltration,[131,228,229] ionic media and pH changes,[230,231] and interaction with special molecules[232]) can be used in various sensing applications (see Fig. 11B, for example).[97,145,173] Designing such bio-inspired sensors to achieve a sensory response within the visible region relies on the relationship between the material properties, their intrinsic nanostructures and the reflected light. Bio-inspired colour sensors within the visible region provide a simple, yet powerful, detection mechanism, which holds great potential for various applications in different industries, including diagnostics,[233,234] environmental monitoring, workplace hazard identification, and threat detection.[235–237] Consequently, there are several review articles focusing on the development of bio-inspired colorimetric sensors, their fabrication methods, their operation mechanisms and the possible industries involved.[89,238–241]

Another system that can also exhibit changes in colour under a wide range of stimuli is the chiral nematic photonic structures. Their use in various sensing applications were also discussed in a recent review.[242] One of he most studied chiral nematic photonic structures is produced through the self-assembly of cellulose nanocrystals and their organic/inorganic composite structures (see section 3.2.1.2). Cellulose is a highly hydrophilic material, and upon exposure to water (in liquid or vapour), the helicoidal pitch of its CNC assembly (hence the colour) shifts reversibly along with the film swelling.[203,243] When the porosity of such compact chiral nematic films is increased through supramolecular methods (using urea formaldehyde, for example), the final mesoporous chiral cellulose material displays dynamic photonic properties, which may make them ideal for optical filters and/or chemical sensors.[244]

4.2 Surface engineering with structurally-coloured systems

The production of photonic arrays, using either top-down or bottom-up strategies, not only produces tunable colours, but also offers a great variety of applications, notably due to the use of advanced surface engineering involved in such processes. It is possible to use a great variety of materials to combine different effects, such as hydrophobicity or electric field-driven colour tunability.

The iridescent and metallic appearances of the structurally coloured species are notably used to attract the attention of potential mates, or to startle predators. An obvious application for these visually attractive, and optically sophisticated, constructions is to create security encoding and anti-counterfeiting features. As we have seen in section 3, replicating these features is indeed highly challenging. Therefore, significant efforts are made to develop security features and encryption applications, by using both top-down and bottom-up strategies. The use of self-assembled dielectric materials offers an accessible way to produce security features.[87,245] Additional optical illusions can be achieved by using different material properties: for example, employing a superparamagnetic iron oxide core (Fe_3O_4) inside SiO_2 colloidal spheres, Kim *et al.*[206] demonstrated the patterning of multiple structural colours with a magnetic field (Fig. 11D). Such systems are also lithographically fixable, which could allow the industrial production of these high-resolution multicoloured patterns.[206] In a similar work, Hu *et al.*[246] used superparamagnetic colloidal particles to produce dual photonic band-gap heterostructures, which showed switchable colour changes upon an applied magnetic field. This process adds another security element for anti-counterfeiting applications.[246] Plasmonic materials, on the other hand, exhibit extraordinary enhancements in confining optical fields with well-controlled intensity, phase and polarisation of light, beyond the diffraction limit.[247] Therefore, these structural colours also hold a great potential in the development of materials for forgery protection.[65,248]

Interestingly, apart from their structural colour, *Morpho* butterflies also attracted much interest due to the excellent water repellency of their wings. This effect is caused by the multiple superhydrophobic ridges, giving them a self-cleaning ability.[249] Replication of structural colouration, together with the "lotus effect" (that is, the self-cleaning effect due to the very high water repellence caused by both the nanostructures and the materials chemistry) was studied by Gu *et al.*[187] in inverse opal systems. In their work, they demonstrate the long-order range organisation, through a bi-component nanoparticles (that is, monodispersed polystyrene spheres, in the range of $300-500$ nm along with silica nanoparticles of size 6 nm) using the vertical convective self-assembly (see section 3.2.1.1). Upon the removal of the polystyrene opal frame, and after the surface modification of the silica inverse opal substrates with a fluoroalkylsilane, they achieved superhydrophobicity with a 155° contact angle.[187] In another study, the same silica inverse opal structure was prepared similarly, but the substrates was covered with azobenzene by electrostatic layer-by-layer self-assembly. Such films showed a reversible change in the wettability of the surface, depending on the applied irradiation, which caused a change in the azobenzene isomeric conformations.[250] The extensive research on production of bio-inspired photonic crystals, with structural colour and tunable wettability has been summarized in a review.[251] On the side of top-down production, Wang *et al.*[252] fabricated periodic grating structures on a graphene oxide (GO) film using two-beam laser interference. The process seemed to simultaneously remove the oxygen groups on GO. With increasing laser power, the contact angle of the surfaces was increased to value of 156.7°.[252] The pillar structures on the surface is usually responsible of the coloration and the hydrophobicity. For the glasswing butterfly *Greta oto*, the small nanopillars covering the transparent regions of its wings actually cause anti-reflection behaviour, which inspires applications for omnidirectional anti-reflective coatings.[253] Moth eyes are also famous examples of anti-reflective structures, and have been subject of extensive biomimetics studies, with promising applications in display technologies, solar panels, and light emitting diodes.[23,254,255]

Patterning the colloidal crystals, or dynamically tuning their periodicity, could potentially be used as a basis for colour displays in reflection mode (Fig. 11C).[116,142,145,221,256,257] Furthermore, the deliberate insertion of organised defects into colloidal crystals, or doping such crystals with light emitters, enables the creation of optical waveguides[258,259] and lasers.[260]

Three-dimensional photonic crystals, based on colloidal self-assembly and inverse opal structures, possess a photonic band-gap based on their intrinsic periodic structure, which can selectively modify the propagation of light with a specific wavelength. Ideally, it may be desired to maximise the coupling of light into a structure, while minimising the amount of light that escapes. Having such control on the propagation of light, and localization of photons, is, without doubt, very beneficial for photocatalytic and photovoltaic applications. Researchers have studied various inverse opal systems that implicate metal oxides such as TiO_2, ZnO, $BiVO_4$ or WO_3, for both dye-sensitised solar cell devices (DSSCs), and as photoanodes in photoelectrochemical cells.[194,261–264] One of the most studied metal oxides in such systems is TiO_2, which is usually applied as a bulk film in DSSCs. The bulk TiO_2 layer scatters and reflects the light randomly, whereas the reflectance of TiO_2 in the inverse opal geometry is highly wavelength-selective. In that case, the incident light could be managed effectively to enhance light harvesting, by matching the electronic band-gap of the metal oxide to its photonic band-gap[194,261], or by matching the photonic band-gap to the absorption of the sensitising dye.[265] Organic-inorganic halide perovskites-based solar cells is yet another class of photovoltaic systems with a photon-to-electron conversion mechanism which is quite different from that of the classical metal oxide solar cells. Henry Snaith's team at the University of Oxford produced perovskite solar cells on a biomimetic scaffold of alternating layers of TiO_2 and porous SiO_2, and demonstrated that it is possible to tune the hue of the perovskite device. Structural coloration in perovskite solar cells is proven to bring many advantages, such as tunability of the colours for specific panchromatic photovoltaic absorbers, and the fact that colouration will not bleach or fade with time offers great stability for such systems.[266]

Nature offers an extended array of nanostructures, with smart selection of cost effective materials to sustain numerous physical functions. In addition to mechanical integrity, colouration and hydrophobicity (section 4.2), the nanostructures originally designed to attain structural colours can also help us to produce highly light-absorbent biomimetic materials. For example, in order to maintain a constant body temperature, the *Troides magellanus* butterfly also exhibits an unusual absorption of visible light (98%), while emitting radiation in the infrared region, due to the special organization of chitin.[267] Possibly, this added functionality is used to dissipate heat for temperature regulation, and is also found in the *Morpho* species.[268] Mimicking the dissipative property of chitin may also be beneficial for photovoltaic applications.

4.3 Structural colours in art, cosmetics, paints and textiles

The list of potential applications for structurally-coloured materials is indeed quite large. Yet, the most obvious way to use these materials is by exploiting the aesthetic aspect of their vivid colouration. Hence, relevant industries, such as art, cosmetics, textiles and decorations, have adopted structural colours to create non-traditional pigments and dyes long ago.

Structurally-coloured species, such as opals, nacre and pearls, have been used in jewelry and the fabrication of decorative items (such as pots, boxes etc.) for centuries.[269] Some recent modern art pieces use the brilliant *Morpho*, and other butterflies, as coloured entities by incorporating entire specimens as themselves (for example, Damien Hirst's "Psalm 6: Domine, ne in furore.", 2008). Artists can take advantage of structural colours to create specific colouration and aesthetic expressions. Some artistic paints' suppliers, such as Golden Artist Colors®,* or Liquitex®,† are producing a large variety of acrylic-based, structurally coloured paints, which impart shimmering iridescent or interference reflective qualities. These usually arise from nanoflakes of mica, coated with a thin layer of titanium dioxide, metal or iron oxide pigments.

But some artists go beyond what is available on the market, in terms of mimicking iridescence effects, and actually create their own structural colours to achieve unique displays.[270,271] Such artists, like Kate Nichols,‡ Paul Evans,§ and Franziska Schenk,¶ usually hold laboratories' artist-in-residence positions, or closely collaborate with scientists, to synthesize their own nanoparticles that mimic various optical effects seen in *Morpho* butterflies, beetles and bird feathers (see Figs. 12A and 12B). This way, they also construct non-reproducible pieces by making their own base materials.

As we have seen in section 3.2, a way to fabricate structural colours is to produce nanoparticles that self-organise. Yet, colloidal self-assembly has several limitations, due to the sensitive nature of the process: the crystal orientation in large scales is not fully controllable, the process is time-consuming, and the success of the self-assembly is heavily dependent on the substrates, where an even colouration can only be achieved on perfectly flat and uniform surfaces. The best way to use the structurally-coloured colloidal crystals as pigments is to process them into a powder form (Fig. 11A).[191] Hence, in order to overcome the shortcomings of solvent-based self-assembly processes, Park *et al.*[272] introduced paintings that produce structural colours by rubbing a nanoparticle powder on an elastomer surface. Their technique is a quick, highly reproducible mean to fabricate a single crystal monolayer assembly of particles over an unlimited area.[272,273]

Pearlescent pigments, on the other hand, can be produced by coating mica particles with thin layers of metal oxides (TiO_2, ZrO_2 or SiO_2) to create lustrous, iridescent and other angle-dependent optical effects. Such pigments are indeed used extensively in a variety of industrial products.[274,275] Similar pearlescent pigments have notably captured the interest of cosmetics' industries. Again inspired by the structural colours of butterfly wings, researchers at L'Oréal®, for example, developed multilayers of mica, silica, and networks of polymers or silica beads with remarkable optical effects. By varying the number of layers, they could achieve different optical effects: with a simple thin layer, they obtained the classical iridescence effect (see section 2.1); but by multiplying the layers of particles or metallic oxides (up to 200 layers), they could produced a mirror effect, where the colour of the light transmitted is complementary to the light reflected.|| Colour-shift, colour-flip or holographic effects on curved surfaces (such as cars) can also be achieved using microflakes and chameleon pearl-based pigments. These can be readily applied onto a car's body, by mixing them with different paint matrices for coating.**††

Further to these new generations of powderous forms of structurally-colouring paints, pre-defined and tuned colloidal suspensions can also be directly used as paints.[276,277] Alternatively, to fabricate a paint composition, photo-curable pre-assembled colloidal photonic crystal films can be ground to microscopic photonic crystal flakes and redispersed into a solvent.[278] Similarly, the aforementioned "photonic balls" (section 3.2.1.1) may be used directly in paint formulations.[279,280] Additionally, it is possible to enhance the colour effect of these opalescent photonic structures, by adding small amounts of highly light-absorbing material, such as carbon, which incorporates in the interstitial space surrounding the high-refractive-index spheres.[281–283]

In textile-related applications, bio-inspired opalescent films can also be produced at industrial scales, by using an edge-shearing method. In this process, colloidal particles are sandwiched as a thin film between two removable polymer sheets, which are then drawn over a sharp edge. This way, the particles rearrange themselves to form a highly periodic structure, greatly strengthening their response to light, and making their colour particularly intense.[284] The edge-shearing process notable permits the rapid

* http://www.goldenpaints.com
† http://www.liquitex.com
‡ http://www.katenicholsstudio.com
§ http://www.pkevans.co.uk
¶ http://www.franziskaschenk.co.uk
|| http://www.loreal.com
** http://www.pearlsandpigments.com
†† http://www.sfxc.co.uk

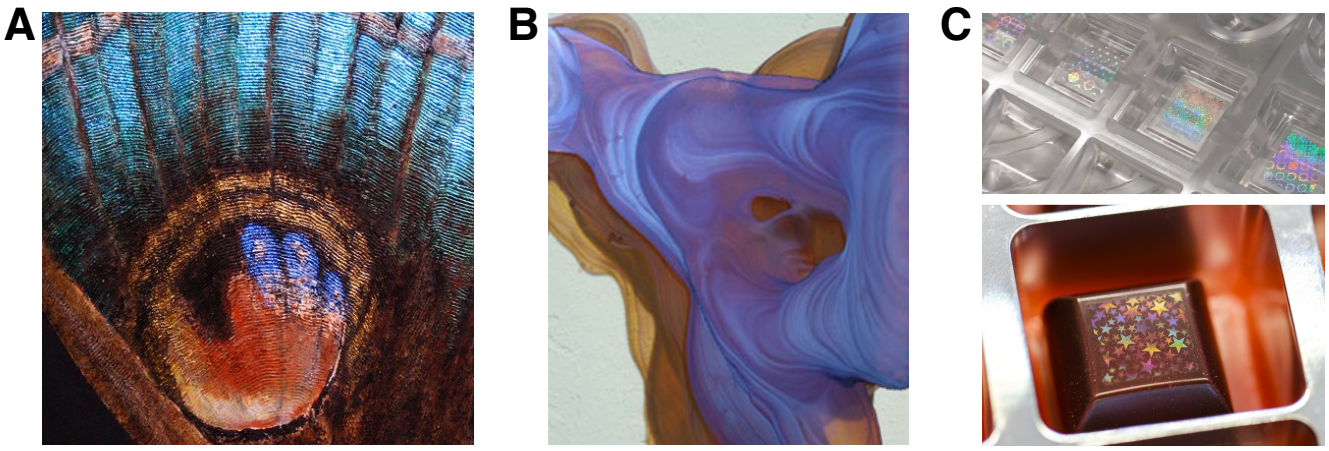

Fig. 12 (A) Franziska Schenk's "Erebus obscura", 2008 uses structurally-coloured paints over a black pigmentary base (reproduced with permission, © 2008 Franziska Schenk). (B) Kate Nichols' "Through the Looking Glass", 2011 employs silver nanoparticles (image courtesy of Kate Nichols). (C) Holographic patterns made from chocolate (bottom), via direct casting with pre-fabricated polycarbonate moulds (top); images courtesy of Morphotonix.

production of large scale films. Along the same lines, researchers at the Nissan Motor Company® demonstrated that it is possible to produce structurally-coloured fibres, and a fabric woven, through a conjugated melt spinning method.[285] In this process, the non-circular and structurally-coloured fibres are notably pre-fabricated, prior to their melt-spinning, by stacking alternating polymer layers with large refractive index contrast. Their colour can be tuned by changing the thicknesses of the constituent polymer layers.

Finally, it is possible to produce colouration on food without using any artificial colouring agents, directly by using the top-down methods. For example, the Swiss nanotechnology company Morphotonix⌗ developed a way to create holographic patterns on the surface of chocolates, without using any chemical additives, by directly casting the chocolate into diffractive holograms (see Fig. 12C). For this purpose, the company developed a technology to micro-pattern bulk, free-form metallic templates employed in the fabrication of the polycarbonate moulds that are subsequently used in chocolate production. The diffractive patterns from the metal are thus replicated into the chocolate during its casting process. Even though the process and design are not directly inspired by nature, the use of an edible substance ostensibly shows the variety of potential materials that could be manufactured into structural colours.

5 Conclusions

The structural colours of living creatures are designed for various types of biological function. They originate from basic optical phenomena, such as diffraction, interference and scattering, which are often finely combined and balanced to optimise the colouration effects for the particular function sought. From an engineering point of view, natural structural colours exhibit attractive features, such as iridescence, polarisation-dependent response, or long-life and high environmental resistance. They also tend to be particularly energy-efficient. For these reasons, the structural colours found in nature have attracted intense research and biomimicry efforts in the recent years.

In this review, we have briefly recalled the physical principles behind structural colours in nature, before focussing on the recent achievements in manufacturing these bio-inspired structures. We also reported the current or potential applications of structural colours in industry, arts and sciences. Currently, the most successful approaches for fabricating structural colours usually associate several top-down and bottom-up processes. Still, these techniques are often limited in terms of consistency, object dimensions and throughput.

We presented strategies using self-assembly in great details in this review (section 3.2.1). Aside from being the fabrication process for most materials found in living species, self-assembly also appears to be the best method for building structured materials that exhibit colouration: firstly, it is both economical (because it typically uses few materials) and environmental-friendly (since the process generally requires little external intervention or additional sources of energy); secondly, it allows for industrial scales production with a high degree of accuracy, in terms of structure conservation and periodicity over large objects.

Controlling self-assembly, however, is an arduous task, which demands further research in chemistry and physics. Additionally, it may be appealing to also mimic the material properties of the natural self-assembling building blocks, such as chitin, cellulose, melanin, etc. Often, in addition to colouration, the nanostructures that are formed from these constituents serve multiple other functions (self-cleaning, heat dissipation, etc.), which are inherited from the building material itself. We have tackled some of these aspects in section 4.2, and showed how multi-functionalities are also an attractive feature for the engineers, over an even wider range of applications (e.g., solar panels, packaging, etc.).

Most strikingly, living creatures employ a very narrow range of materials, when compared with the variety of materials composing synthetic functional objects. The optimisation in the materials selection found in nature should also be a good of inspiration for future manufacturing strategies. Natural substances used for

⌗ http://www.morphotonix.com

structural colours in living species, in particular, are abundant, sustainable and safe for the environment. They may as well be used as the basis for bio-inspired structured materials. But they may also form the basis for future custom-designed structures that go beyond what is found in nature.

Hence, not only the structural arrangements, but also the fabricating processes and materials may be biologically inspired. A concerted effort, across many disciplines, is needed to master the reproduction of the highly efficient designs and processes found in nature. But this is an essential step to undertake in order to further invent our own structured materials. Much is left to investigate, and this field of research is indeed rapidly growing, as nature's evolutionary engineering is progressively elucidated.

Acknowledgements

We thank Dr Ian Parry, Dr Veronica Savu and Dr Silvia Vignolini for their comments on the manuscript.

References

1 A. R. Parker, *J. Opt. A: Pure Appl. Opt.*, 2000, **2**, R15–R28.
2 S. Kinoshita, *Structural Colors in the Realm of Nature*, World Scientific, Singapore, 2008.
3 J. Sun, B. Bhushan and J. Tong, *RSC Adv.*, 2013, **3**, 14862–14889.
4 S. Kinoshita, S. Yoshioka and J. Miyazaki, *Rep. Prog. Phys.*, 2008, **71**, 076401.
5 T. F. Anderson and A. G. Richards Jr., *J. Appl. Phys.*, 1942, **13**, 748–758.
6 E. Yablonovitch, *Phys. Rev. Lett.*, 1987, **58**, 2059–2062.
7 J. D. Joannopoulos, S. G. Johnson, J. N. Winn and R. D. Meade, *Photonic Crystals: Molding the Flow of Light*, Princeton University Press, Princeton, 2nd edn, 2008.
8 F. P. Barrows and M. H. Bartl, *Nanomater. Nanotechnol.*, 2014, **4**, 1.
9 M. J. Madou, *Fundamentals of Microfabrication and Nanotechnology*, CRC Press, Boca Raton, 3rd edn, 2012.
10 M. F. Land, *Prog. Biophys. Mol. Biol.*, 1972, **24**, 75–106.
11 M. Srinivasarao, *Chem. Rev.*, 1999, **99**, 1935–1961.
12 A. R. Parker, *Mater. Today*, 2002, **5**, 26–31.
13 P. Vukusic and J. R. Sambles, *Nature*, 2003, **424**, 852–855.
14 A. R. Parker, *Phil. Trans. R. Soc. A*, 2004, **362**, 2709–2720.
15 L. P. Lee and R. Szema, *Science*, 2005, **310**, 1148–1150.
16 A. R. Parker and H. E. Townley, *Nat. Nanotechnol.*, 2007, **2**, 347–353.
17 S. M. Doucet and M. G. Meadows, *J. R. Soc. Interface*, 2009, **6**, S115–S132.
18 A. R. Parker, *Phil. Trans. R. Soc. A*, 2009, **367**, 1759–1782.
19 J.-P. Vigneron and P. Simonis, *Adv. Insect Physiol.*, 2010, **38**, 181–218.
20 P. V. Braun, *Nature*, 2011, **472**, 423–424.
21 H. Fudouzi, *Sci. Technol. Adv. Mater.*, 2011, **12**, 064704.
22 Y. Zhao, Z. Xie, H. Gu, C. Zhu and Z. Gu, *Chem. Soc. Rev.*, 2012, **41**, 3297–3317.
23 A. Saito, *Sci. Technol. Adv. Mater.*, 2011, **12**, 064709.
24 J. Xu and Z. Guo, *J. Colloid Interface Sci.*, 2013, **406**, 1–17.
25 M. Kolle, *PhD thesis*, University of Cambridge, 2010.
26 *Biomimetics in Photonics*, ed. O. Karthaus, CRC Press, Boca Raton, 2012.
27 *Photobiology: The Science of Light and Life*, ed. L. O. Björn, Springer, New York, 3rd edn, 2015.
28 D. Zhang, W. Zhang, J. Gu, T. Fan, Q. Liu, H. Su and S. Zhu, *Prog. Mater. Sci.*, 2015, **68**, 67–96.
29 Y. Fu, C. A. Tippets, E. U. Donev and R. Lopez, *WIREs Nanomed. Nanobiotechnol.*, 2016, 10.1002–wnan.1396.
30 M. Born and E. Wolf, *Principles of Optics*, Pergamon, Oxford, 6th edn, 1980.
31 H. A. Macleod, *Thin-Film Optical Filters* , CRC Press, Boca Raton, 4th edn, 2010.
32 H. M. Whitney, M. Kolle, P. Andrew, L. Chittka, U. Steiner and B. J. Glover, *Science*, 2009, **323**, 130–133.
33 A. L. Ingram, V. Lousse, A. R. Parker and J.-P. Vigneron, *J. R. Soc. Interface*, 2008, **5**, 1387–1390.
34 T. L. Tan, D. Wong and P. Lee, *Opt. Express*, 2004, **12**, 4847–4854.
35 Z. Knittl, *Optics of Thin Films*, Wiley, London, 1976.
36 H. de Vries, *Acta Crystallogr.*, 1951, **4**, 219–226.
37 E. Shevtsova, C. Hansson, D. H. Janzen and J. Kjærandsen, *Proc. Natl. Acad. Sci. U.S.A.*, 2011, **108**, 668–673.
38 S. Yoshioka, E. Nakamura and S. Kinoshita, *J. Phys. Soc. Jpn.*, 2007, **76**, 013801.
39 R. Maia, J. V. O. Caetano, S. N. Báo and R. H. Macedo, *J. R. Soc. Interface*, 2009, **6**, S203–S211.
40 A. E. Seago, P. Brady, J.-P. Vigneron and T. D. Schultz, *J. R. Soc. Interface*, 2009, **6**, S165–S184.
41 V. Sharma, M. Crne, J. O. Park and M. Srinivasarao, *Science*, 2009, **325**, 449–451.
42 D. G. Stavenga, H. L. Leertouwer, N. J. Marshall and D. Osorio, *Proc. R. Soc. B*, 2011, **278**, 2098–2104.
43 S. Yoshioka, B. Matsuhana, S. Tanaka, Y. Inouye, N. Oshima and S. Kinoshita, *J. R. Soc. Interface*, 2011, **8**, 56–66.
44 D. J. Brink, N. G. van der Berg and A. J. Botha, *Appl. Opt.*, 2002, **41**, 717–722.
45 L. M. Mäthger, E. J. Denton, N. J. Marshall and R. T. Hanlon, *J. R. Soc. Interface*, 2009, **6**, S149–S163.
46 S. Vignolini, P. J. Rudall, A. V. Rowland, A. Reed, E. Moyroud, R. B. Faden, J. J. Baumberg, B. J. Glover and U. Steiner, *Proc. Natl. Acad. Sci. U.S.A.*, 2012, **109**, 15712–15715.
47 K. Sakoda, *Optical Properties of Photonic Crystals*, Springer, Berlin, 2nd edn, 2005, vol. 80.
48 J.-M. Lourtioz, H. Benisty, V. Berger, J.-M. Gérard, D. Maystre, A. Tchelnokov and D. Pagnoux, *Photonic Crystals: Towards Nanoscale Photonic Devices*, Springer, Berlin, 2nd edn, 2008.
49 I. A. Sukhoivanov and I. V. Guryev, *Photonic Crystals: Physics and Practical Modeling*, Springer, Heidelberg, 2009, vol. 152.
50 E. Pavarini, L. C. Andreani, C. Soci, M. Galli, F. Marabelli and D. Comoretto, *Phys. Rev. B*, 2005, **72**, 045102.

51 T. M. Trzeciak and P. Vukusic, *Phys. Rev. E*, 2009, **80**, 061908.

52 J. Zi, X. Yu, Y. Li, X. Hu, C. Xu, X. Wang, X. Liu and R. Fu, *Proc. Natl. Acad. Sci. U.S.A.*, 2003, **100**, 12576–12578.

53 E. Lee, J. Miyazaki, S. Yoshioka, H. Lee and S. Sugita, *Ornithol. Sci.*, 2012, **11**, 59–64.

54 J. V. Sanders, *Nature*, 1964, **204**, 1151–1153.

55 J. W. Galusha, L. R. Richey, J. S. Gardner, J. N. Cha and M. H. Bartl, *Phys. Rev. E*, 2008, **77**, 050904.

56 V. Saranathan, C. O. Osuji, S. G. J. Mochrie, H. Noh, S. Narayanan, A. Sandy, E. R. Dufresne and R. O. Prum, *Proc. Natl. Acad. Sci. U.S.A.*, 2010, **107**, 11676–11681.

57 J.-P. Vigneron and P. Simonis, *Physica B*, 2012, **407**, 4032–4036.

58 B. D. Wilts, K. Michielsen, H. De Raedt and D. G. Stavenga, *J. R. Soc. Interface*, 2012, **9**, 1609–1614.

59 C. F. Bohren and D. R. Huffman, *Absorption and Scattering of Light by Small Particles*, Wiley, Weinheim, 1998.

60 H. Noh, S. F. Liew, V. Saranathan, S. G. J. Mochrie, R. O. Prum, E. R. Dufresne and H. Cao, *Adv. Mater.*, 2010, **22**, 2871–2880.

61 R. O. Prum, E. R. Dufresne, T. Quinn and K. Waters, *J. R. Soc. Interface*, 2009, **6**, S253–S265.

62 P. Vukusic, B. Hallam and J. Noyes, *Science*, 2007, **315**, 348–348.

63 M. Burresi, L. Cortese, L. Pattelli, M. Kolle, P. Vukusic, D. S. Wiersma, U. Steiner and S. Vignolini, *Sci. Rep.*, 2014, **4**, 6075.

64 J. T. Bagnara, P. J. Fernandez and R. Fujii, *Pigment Cell Res.*, 2007, **20**, 14–26.

65 K. Kumar, H. Duan, R. S. Hegde, S. C. W. Koh, J. N. Wei and J. K. W. Yang, *Nat. Nanotechnol.*, 2012, **7**, 557–561.

66 E. Cazetta, L. S. Zumstein, T. A. Melo-Júnior and M. Galetti, *Braz. J. Bot.*, 2008, **31**, 303–308.

67 M. Kolle, A. Lethbridge, M. Kreysing, J. J. Baumberg, J. Aizenberg and P. Vukusic, *Adv. Mater.*, 2013, **25**, 2239–2245.

68 E. Van Hooijdonk, S. Berthier and J.-P. Vigneron, *J. Appl. Phys.*, 2012, **112**, 074702.

69 S. Mouchet, J.-P. Vigneron, J.-F. Colomer, C. Vandenbem and O. Deparis, Proc. SPIE, 2012, p. 848003.

70 P. Vukusic, J. R. Sambles and C. R. Lawrence, *Nature*, 2000, **404**, 457–457.

71 Y.-Y. Diao and X.-Y. Liu, *Opt. Express*, 2011, **19**, 9232–9241.

72 M. D. Shawkey, N. I. Morehouse and P. Vukusic, *J. R. Soc. Interface*, 2009, **6**, S221–S231.

73 A. Saito, M. Nakajima, Y. Miyamura, K. Sogo, Y. Ishikawa and Y. Hirai, Proc. SPIE, 2006, p. 63270Z.

74 E. R. Dufresne, H. Noh, V. Saranathan, S. G. J. Mochrie, H. Cao and R. O. Prum, *Soft Matter*, 2009, **5**, 1792–1795.

75 S. Kinoshita, S. Yoshioka and K. Kawagoe, *Proc. R. Soc. B*, 2002, **269**, 1417–1421.

76 R. O. Prum, T. Quinn and R. H. Torres, *J. Exp. Biol.*, 2006, **209**, 748–765.

77 P. Vukusic, J. R. Sambles, C. R. Lawrence and R. J. Wootton, *Proc. R. Soc. B*, 1999, **266**, 1403–1411.

78 C. Gower, *The Auk*, 1936, **53**, 178–185.

79 D. G. Stavenga, H. L. Leertouwer, D. C. Osorio and B. D. Wilts, *Light Sci. Appl.*, 2015, **4**, e243.

80 A. J. Parnell, A. L. Washington, O. O. Mykhaylyk, C. J. Hill, A. Bianco, S. L. Burg, A. J. C. Dennison, M. Snape, A. J. Cadby, A. Smith, S. Prevost, D. M. Whittaker, R. A. L. Jones, J. P. A. Fairclough and A. R. Parker, *Sci. Rep.*, 2015, **5**, 18317.

81 A. Finnemore, P. Cunha, T. Shean, S. Vignolini, S. Guldin, M. Oyen and U. Steiner, *Nat. Commun.*, 2012, **3**, 966.

82 M. Liesegang and R. Milke, *Am. Mineral.*, 2014, **99**, 1488–1499.

83 K. Yu, T. Fan, S. Lou and D. Zhang, *Prog. Mater. Sci.*, 2013, **58**, 825–873.

84 A. Pimpin and W. Srituravanich, *Eng. J.*, 2012, **16**, 37–55.

85 M. Maldovan and E. L. Thomas, *Periodic Materials and Interference Lithography*, Wiley, Weinheim, 2009.

86 N. Kooy, K. Mohamed, L. T. Pin and O. S. Guan, *Nanoscale Res. Lett.*, 2014, **9**, 320.

87 H. S. Lee, T. S. Shim, H. Hwang, S.-M. Yang and S.-H. Kim, *Chem. Mater.*, 2013, **25**, 2684–2690.

88 M. A. Mohammad, M. Muhammad, S. K. Dew and M. Stepanova, *Nanofabrication*, Springer, Vienna, 2012, pp. 11–41.

89 I. B. Burgess, M. Lončar and J. Aizenberg, *J. Mater. Chem. B*, 2013, **1**, 6075–6086.

90 J.-H. Jang, C. K. Ullal, M. Maldovan, T. Gorishnyy, S. Kooi, C. Y. Koh and E. L. Thomas, *Adv. Funct. Mater.*, 2007, **17**, 3027–3041.

91 R. H. Siddique, R. Hünig, A. Faisal, U. Lemmer and H. Hölscher, *Opt. Mater. Express*, 2015, **5**, 996–1005.

92 T. S. Kustandi, H. Y. Low, J. H. Teng, I. Rodriguez and R. Yin, *Small*, 2009, **5**, 574–578.

93 S. Zhang and Y. Chen, *Sci. Rep.*, 2015, **5**, 16637.

94 T. Balla, S. M. Spearing and A. Monk, *J. Phys. D: Appl. Phys.*, 2008, **41**, 174001.

95 S. H. Ahn and L. J. Guo, *Adv. Mater.*, 2008, **20**, 2044–2049.

96 T.-H. Wong, M. C. Gupta, B. Robins and T. L. Levendusky, *Opt. Lett.*, 2003, **28**, 2342–2344.

97 S. Y. Choi, M. Mamak, G. von Freymann, N. Chopra and G. A. Ozin, *Nano Lett.*, 2006, **6**, 2456–2461.

98 M. E. Calvo, S. Colodrero, T. C. Rojas, J. A. Anta, M. Ocaña and H. Míguez, *Adv. Funct. Mater.*, 2008, **18**, 2708–2715.

99 M. C. Fuertes, F. J. López-Alcaraz, M. C. Marchi, H. E. Troiani, V. Luca, H. Míguez and G. J. A. A. Soler-Illia, *Adv. Funct. Mater.*, 2007, **17**, 1247–1254.

100 T. Scharf, S. Jaquet, P. Ruffieux and H. P. Herzig, *Jpn. J. Appl. Phys.*, 2008, **47**, 6699–6705.

101 J. D. Rancourt, *Optical Thin Films: User Handbook*, SPIE Press, Bellingham, 1996.

102 M. Karaman, S. E. Kooi and K. K. Gleason, *Chem. Mater.*, 2008, **20**, 2262–2267.

103 R. W. Johnson, A. Hultqvist and S. F. Bent, *Mater. Today*, 2014, **17**, 236–246.

104 M. Kolle, P. M. Salgard-Cunha, M. R. J. Scherer, F. Huang, P. Vukusic, S. Mahajan, J. J. Baumberg and U. Steiner, *Nat. Nanotechnol.*, 2010, **5**, 511–515.

105 D. G. Stavenga, B. D. Wilts, H. L. Leertouwer and T. Hariyama, *Phil. Trans. R. Soc. B*, 2011, **366**, 709–723.

106 P. Tzeng, D. J. Hewson, P. Vukusic, S. J. Eichhorn and J. C. Grunlan, *J. Mater. Chem. C*, 2015, **3**, 4260–4264.

107 K. Chung, S. Yu, C.-J. Heo, J. W. Shim, S.-M. Yang, M. G. Han, H.-S. Lee, Y. Jin, S. Y. Lee, N. Park and J. H. Shin, *Adv. Mater.*, 2012, **24**, 2375–2379.

108 M. Yaman, T. Khudiyev, E. Ozgur, M. Kanik, O. Aktas, E. O. Ozgur, H. Deniz, E. Korkut and M. Bayindir, *Nat. Mater.*, 2011, **10**, 494–501.

109 T. Khudiyev, E. Ozgur, M. Yaman and M. Bayindir, *Nano Lett.*, 2011, **11**, 4661–4665.

110 T. Khudiyev, T. Dogan and M. Bayindir, *Sci. Rep.*, 2014, **4**, 4718.

111 A. Saito, Y. Ishikawa, Y. Miyamura, M. Akai-kasaya and Y. Kuwahara, Proc. SPIE, 2007, p. 676706.

112 J. F. Galisteo-López, M. Ibisate, R. Sapienza, L. S. Froufe-Pérez, Á. Blanco and C. López, *Adv. Mater.*, 2011, **23**, 30–69.

113 S.-H. Kim, S. Y. Lee, S.-M. Yang and G.-R. Yi, *NPG Asia Mater.*, 2011, **3**, 25–33.

114 V. N. Astratov, V. N. Bogomolov, A. A. Kaplyanskii, A. V. Prokofiev, L. A. Samoilovich, S. M. Samoilovich and Y. A. Vlasov, *Nuovo Cimento D*, 1995, **17**, 1349–1354.

115 J. Sussman, D. Snoswell, A. Kontogeorgos, J. J. Baumberg and P. Spahn, *Appl. Phys. Lett.*, 2009, **95**, 173116.

116 L. Mishchenko, B. Hatton, M. Kolle and J. Aizenberg, *Small*, 2012, **8**, 1904–1911.

117 C. E. Finlayson and J. J. Baumberg, *Polym. Int.*, 2013, **62**, 1403–1407.

118 Y. Takeoka, S. Yoshioka, A. Takano, S. Arai, K. Nueangnoraj, H. Nishihara, M. Teshima, Y. Ohtsuka and T. Seki, *Angew. Chem. Int. Ed.*, 2013, **52**, 7261–7265.

119 Y. Takeoka, *J. Mater. Chem. C*, 2013, **1**, 6059–6074.

120 R. Mayoral, J. Requena, J. S. Moya, C. López, A. Cintas, H. Míguez, F. Meseguer, L. Vázquez, M. Holgado and Á. Blanco, *Adv. Mater.*, 1997, **9**, 257–260.

121 M. Holgado, F. García-Santamaría, A. Blanco, M. Ibisate, A. Cintas, H. Míguez, C. J. Serna, C. Molpeceres, J. Requena, A. Mifsud, F. Meseguer and C. López, *Langmuir*, 1999, **15**, 4701–4704.

122 S. H. Park, D. Qin and Y. Xia, *Adv. Mater.*, 1998, **10**, 1028–1032.

123 A. S. Dimitrov and K. Nagayama, *Langmuir*, 1996, **12**, 1303–1311.

124 P. Jiang, J. F. Bertone, K. S. Hwang and V. L. Colvin, *Chem. Mater.*, 1999, **11**, 2132–2140.

125 O. L. J. Pursiainen, J. J. Baumberg, H. Winkler, B. Viel, P. Spahn and T. Ruhl, *Opt. Express*, 2007, **15**, 9553–9561.

126 P. Spahn, C. E. Finlayson, W. Mbi Etah, D. R. E. Snoswell, J. J. Baumberg and G. P. Hellmann, *J. Mater. Chem.*, 2011, **21**, 8893–8897.

127 S. Magkiriadou, J.-G. Park, Y.-S. Kim and V. N. Manoharan, *Opt. Mater. Express*, 2012, **2**, 1343–1352.

128 L. Zulian, E. Emilitri, G. Scavia, C. Botta, M. Colombo and S. Destri, *ACS Appl. Mater. Interfaces*, 2012, **4**, 6071–6079.

129 Y. Zhao, L. Shang, Y. Cheng and Z. Gu, *Acc. Chem. Res.*, 2014, **47**, 3632–3642.

130 K. Xu, J.-H. Xu, Y.-C. Lu and G.-S. Luo, *Cryst. Growth Des.*, 2013, **13**, 926–935.

131 S.-N. Yin, C.-F. Wang, S.-S. Liu and S. Chen, *J. Mater. Chem. C*, 2013, **1**, 4685–4690.

132 H. Gu, Y. Zhao, Y. Cheng, Z. Xie, F. Rong, J. Li, B. Wang, D. Fu and Z. Gu, *Small*, 2013, **9**, 2266–2271.

133 J. Hu, X.-W. Zhao, Y.-J. Zhao, J. Li, W.-Y. Xu, Z.-Y. Wen, M. Xu and Z.-Z. Gu, *J. Mater. Chem.*, 2009, **19**, 5730–5736.

134 T. Kanai, D. Lee, H. C. Shum and D. A. Weitz, *Small*, 2010, **6**, 807–810.

135 Y. Zhao, Y. Cheng, L. Shang, J. Wang, Z. Xie and Z. Gu, *Small*, 2014, **11**, 151–174.

136 N. Vogel, S. Utech, G. T. England, T. Shirman, K. R. Phillips, N. Koay, I. B. Burgess, M. Kolle, D. A. Weitz and J. Aizenberg, *Proc. Natl. Acad. Sci. U.S.A.*, 2015, **112**, 10845–10850.

137 J. D. Simon and D. N. Peles, *Acc. Chem. Res.*, 2010, **43**, 1452–1460.

138 M. Xiao, Y. Li, M. C. Allen, D. D. Deheyn, X. Yue, J. Zhao, N. C. Gianneschi, M. D. Shawkey and A. Dhinojwala, *ACS Nano*, 2015, **9**, 5454–5460.

139 J. Wang, L. Yang, D. Lin, Y. Luo, D. Li and Q. Meng, *J. Chem. Phys.*, 2012, **137**, 234111.

140 A. J. Kim, R. Scarlett, P. L. Biancaniello, T. Sinno and J. C. Crocker, *Nat. Mater.*, 2009, **8**, 52–55.

141 S.-M. Yang, S.-H. Kim, J.-M. Lim and G.-R. Yi, *J. Mater. Chem.*, 2008, **18**, 2177–2190.

142 S. Y. Lee, S.-H. Kim, H. Hwang, J. Y. Sim and S.-M. Yang, *Adv. Mater.*, 2014, **26**, 2391–2397.

143 M. Schaffner, G. England, M. Kolle, J. Aizenberg and N. Vogel, *Small*, 2015, **11**, 4334–4340.

144 I. B. Burgess, J. Aizenberg and M. Lončar, *Bioinspir. Biomim.*, 2013, **8**, 045004.

145 T. Ding, S. K. Smoukov and J. J. Baumberg, *Nanoscale*, 2015, **7**, 1857–1863.

146 F. M. van der Kooij, K. Kassapidou and H. N. W. Lekkerkerker, *Nature*, 2000, **406**, 868–871.

147 L. Onsager, *Ann. N. Y. Acad. Sci.*, 1949, **51**, 627–659.

148 J.-F. Revol, L. Godbout and D. G. Gray, *J. Pulp Pap. Sci.*, 1998, **24**, 146–149.

149 M. Hasani, E. D. Cranston, G. Westman and D. G. Gray, *Soft Matter*, 2008, **4**, 2238–2244.

150 X. M. Dong, T. Kimura, J.-F. Revol and D. G. Gray, *Langmuir*, 1996, **12**, 2076–2082.

151 J. Pan, W. Hamad and S. K. Straus, *Macromolecules*, 2010, **43**, 3851–3858.

152 S. Beck, J. Bouchard and R. Berry, *Biomacromolecules*, 2011, **12**, 167–172.

153 A. G. Dumanli, H. M. van der Kooij, G. Kamita, E. Reisner, J. J. Baumberg, U. Steiner and S. Vignolini, *ACS Appl. Mater. Interfaces*, 2014, **6**, 12302–12306.

154 A. G. Dumanli, G. Kamita, J. Landman, H. van der Kooij, B. J. Glover, J. J. Baumberg, U. Steiner and S. Vignolini, *Adv. Optical Mater.*, 2014, **2**, 646–650.

155 J.-F. Revol and R. H. Marchessault, *Int. J. Biol. Macromol.*, 1993, **15**, 329–335.

156 T. P. Lodge, *Macromol. Chem. Phys.*, 2003, **204**, 265–273.

157 E. W. Cochran, C. J. Garcia-Cervera and G. H. Fredrickson, *Macromolecules*, 2006, **39**, 2449–2451.

158 M. R. J. Scherer, *PhD thesis*, University of Cambridge, 2013.

159 M. Stefik, S. Guldin, S. Vignolini, U. Wiesner and U. Steiner, *Chem. Soc. Rev.*, 2015, **44**, 5076–5091.

160 C. Mille, E. C. Tyrode and R. W. Corkery, *Chem. Commun.*, 2011, **47**, 9873–9875.

161 T. Deng, C. Chen, C. Honeker and E. L. Thomas, *Polymer*, 2003, **44**, 6549–6553.

162 Y.-W. Chiang, C.-Y. Chou, C.-S. Wu, E.-L. Lin, J. Yoon and E. L. Thomas, *Macromolecules*, 2015, **48**, 4004–4011.

163 A. Matsushita and S. Okamoto, *Macromolecules*, 2014, **47**, 7169–7177.

164 A. C. Edrington, A. M. Urbas, P. DeRege, C. X. Chen, T. M. Swager, N. Hadjichristidis, M. Xenidou, L. J. Fetters, J. D. Joannopoulos, Y. Fink and E. L. Thomas, *Adv. Mater.*, 2001, **13**, 421–425.

165 A. M. Urbas, R. Sharp, Y. Fink, E. L. Thomas, M. Xenidou and L. J. Fetters, *Adv. Mater.*, 2000, **12**, 812–814.

166 S. Valkama, H. Kosonen, J. Ruokolainen, T. Haatainen, M. Torkkeli, R. Serimaa, G. ten Brinke and O. Ikkala, *Nat. Mater.*, 2004, **3**, 872–876.

167 K. Hwang, D. Kwak, C. Kang, D. Kim, Y. Ahn and Y. Kang, *Angew. Chem. Int. Ed.*, 2011, **50**, 6311–6314.

168 S. E. Shin, S. Y. Kim and D. M. Shin, Proc. SPIE, 2010, p. 75991K.

169 H. J. Kim and D. M. Shin, *J. Nanosci. Nanotechnol.*, 2014, **14**, 6235–6237.

170 J. Y. Lim, J. H. Yun, D. b. Jang and D. M. Shin, Proc. SPIE, 2015, p. 958611.

171 T. J. Park, S. K. Hwang, S. Park, S. H. Cho, T. H. Park, B. Jeong, H. S. Kang, D. Y. Ryu, J. Huh, E. L. Thomas and C. Park, *ACS Nano*, 2015, **9**, 12158–12167.

172 J.-H. Lee, C. Y. Koh, J. P. Singer, S.-J. Jeon, M. Maldovan, O. Stein and E. L. Thomas, *Adv. Mater.*, 2014, **26**, 532–569.

173 S. Zhu, X. Liu, Z. Chen, C. Liu, C. Feng, J. Gu, Q. Liu and D. Zhang, *J. Mater. Chem.*, 2010, **20**, 9126–9132.

174 M. R. Weatherspoon, Y. Cai, M. Crne, M. Srinivasarao and K. H. Sandhage, *Angew. Chem. Int. Ed.*, 2008, **47**, 7921–7923.

175 K. E. Shopsowitz, H. Qi, W. Y. Hamad and M. J. MacLachlan, *Nature*, 2010, **468**, 422–425.

176 Y. Vasquez, M. Kolle, L. Mishchenko, B. D. Hatton and J. Aizenberg, *ACS Photonics*, 2014, **1**, 53–60.

177 J. Huang, X. Wang and Z. L. Wang, *Nano Lett.*, 2006, **6**, 2325–2331.

178 G. Cook, P. L. Timms and C. Göltner-Spickermann, *Angew. Chem. Int. Ed.*, 2003, **42**, 557–559.

179 J. C. Hulteen and C. R. Martin, *J. Mater. Chem.*, 1997, **7**, 1075–1087.

180 F. Liu, Y. Liu, L. Huang, X. Hu, B. Dong, W. Shi, Y. Xie and X. Ye, *Opt. Commun.*, 2011, **284**, 2376–2381.

181 Y. Liu, L. Huang and W. Z. Shi, *Adv. Mater. Res.*, 2011, **391-392**, 409–417.

182 D. P. Gaillot, O. Deparis, V. Welch, B. K. Wagner, J.-P. Vigneron and C. J. Summers, *Phys. Rev. E*, 2008, **78**, 031922.

183 W. Zhang, D. Zhang, T. Fan, J. Ding, Q. Guo and H. Ogawa, *Microporous Mesoporous Mater.*, 2006, **92**, 227–233.

184 Y. Chen, J. Gu, S. Zhu, T. Fan, D. Zhang and Q. Guo, *Appl. Phys. Lett.*, 2009, **94**, 053901.

185 A. Stein and R. C. Schroden, *Curr. Opin. Solid State Mater. Sci.*, 2001, **5**, 553–564.

186 C. I. Aguirre, E. Reguera and A. Stein, *Adv. Funct. Mater.*, 2010, **20**, 2565–2578.

187 Z.-Z. Gu, H. Uetsuka, K. Takahashi, R. Nakajima, H. Onishi, A. Fujishima and O. Sato, *Angew. Chem. Int. Ed.*, 2003, **42**, 894–897.

188 K. R. Phillips, N. Vogel, Y. Hu, M. Kolle, C. C. Perry and J. Aizenberg, *Chem. Mater.*, 2014, **26**, 1622–1628.

189 O. Sato, S. Kubo and Z.-Z. Gu, *Acc. Chem. Res.*, 2009, **42**, 1–10.

190 G. I. N. Waterhouse, W.-T. Chen, A. Chan, H. Jin, D. Sun-Waterhouse and B. C. C. Cowie, *J. Phys. Chem. C*, 2015, **119**, 6647–6659.

191 D. P. Josephson, M. Miller and A. Stein, *Z. Anorg. Allg. Chem.*, 2014, **640**, 655–662.

192 B. H. Juárez, P. D. García, D. Golmayo, A. Blanco and C. López, *Adv. Mater.*, 2005, **17**, 2761–2765.

193 H. Míguez, E. Chomski, F. García-Santamaría, M. Ibisate, S. John, C. López, F. Meseguer, J. P. Mondia, G. A. Ozin, O. Toader and H. M. van Driel, *Adv. Mater.*, 2001, **13**, 1634–1637.

194 L. Liu, S. K. Karuturi, L. T. Su and A. I. Y. Tok, *Energy Environ. Sci.*, 2011, **4**, 209–215.

195 M. Liu, X. Li, S. K. Karuturi, A. I. Y. Tok and H. J. Fan, *Nanoscale*, 2012, **4**, 1522–1528.

196 H. Míguez, F. Meseguer, C. López, F. López-Tejeira and J. Sánchez-Dehesa, *Adv. Mater.*, 2001, **13**, 393–396.

197 S. Kim, A. N. Mitropoulos, J. D. Spitzberg, H. Tao, D. L. Kaplan and F. G. Omenetto, *Nat. Photonics*, 2012, **6**, 818–823.

198 A. A. Chabanov, Y. Jun and D. J. Norris, *Appl. Phys. Lett.*, 2004, **84**, 3573–3575.

199 S. Wong, V. Kitaev and G. A. Ozin, *J. Am. Chem. Soc.*, 2003, **125**, 15589–15598.

200 B. Hatton, L. Mishchenko, S. Davis, K. H. Sandhage and J. Aizenberg, *Proc. Natl. Acad. Sci. U.S.A.*, 2010, **107**, 10354–10359.

201 E. Dujardin, M. Blaseby and S. Mann, *J. Mater. Chem.*, 2003, **13**, 696–699.

202 A. Ivanova, D. Fattakhova-Rohlfing, B. E. Kayaalp, J. Rathouský and T. Bein, *J. Am. Chem. Soc.*, 2014, **136**, 5930–5937.

203 K. E. Shopsowitz, W. Y. Hamad and M. J. MacLachlan, *J. Am. Chem. Soc.*, 2012, **134**, 867–870.

204 M. K. Khan, W. Y. Hamad and M. J. MacLachlan, *Adv. Mater.*, 2014, **26**, 2323–2328.

205 C. C. Y. Cheung, M. Giese, J. A. Kelly, W. Y. Hamad and M. J. MacLachlan, *ACS Macro Lett.*, 2013, **2**, 1016–1020.

206 H. Kim, J. Ge, J. Kim, S.-e. Choi, H. Lee, H. Lee, W. Park, Y. Yin and S. Kwon, *Nat. Photonics*, 2009, **3**, 534–540.

207 T. Caro, *BioScience*, 2005, **55**, 125–136.

208 Y. Cho, S. Y. Lee, L. Ellerthorpe, G. Feng, G. Lin, G. Wu, J. Yin and S. Yang, *Adv. Funct. Mater.*, 2015, **25**, 6041–6049.

209 C. G. Schäfer, B. Viel, G. P. Hellmann, M. Rehahn and M. Gallei, *ACS Appl. Mater. Interfaces*, 2013, **5**, 10623–10632.

210 C. G. Schäfer, T. Winter, S. Heidt, C. Dietz, T. Ding, J. J. Baumberg and M. Gallei, *J. Mater. Chem. C*, 2015, **3**, 2204–2214.

211 B. Viel, T. Ruhl and G. P. Hellmann, *Chem. Mater.*, 2007, **19**, 5673–5679.

212 L. Duan, B. You, L. Wu and M. Chen, *J. Colloid Interface Sci.*, 2011, **353**, 163–168.

213 E. P. Chan, J. J. Walish, A. M. Urbas and E. L. Thomas, *Adv. Mater.*, 2013, **25**, 3934–3947.

214 X. Jia, J. Wang, K. Wang and J. Zhu, *Langmuir*, 2015, **31**, 8732–8737.

215 X. Sun, J. Zhang, X. Lu, X. Fang and H. Peng, *Angew. Chem. Int. Ed.*, 2015, **54**, 3630–3634.

216 S. Shang, Z. Liu, Q. Zhang, H. Wang and Y. Li, *J. Mater. Chem. A*, 2015, **3**, 11093–11097.

217 J. Zhang, S. He, L. Liu, G. Guan, X. Lu, X. Sun and H. Peng, *J. Mater. Chem. C*, 2016, **4**, 2127–2133.

218 Y. Hu, L. He and Y. Yin, *Small*, 2012, **8**, 3795–3799.

219 L. He, M. Wang, J. Ge and Y. Yin, *Acc. Chem. Res.*, 2012, **45**, 1431–1440.

220 M. Wang, L. He, W. Xu, X. Wang and Y. Yin, *Angew. Chem. Int. Ed.*, 2015, **54**, 7077–7081.

221 A. C. Arsenault, D. P. Puzzo, I. Manners and G. A. Ozin, *Nat. Photonics*, 2007, **1**, 468–472.

222 T. S. Shim, S.-H. Kim, J. Y. Sim, J.-M. Lim and S.-M. Yang, *Adv. Mater.*, 2010, **22**, 4494–4498.

223 A. A. Shah, M. Ganesan, J. Jocz and M. J. Solomon, *ACS Nano*, 2014, **8**, 8095–8103.

224 B. Michaelis, D. R. E. Snoswell, N. A. W. Bell, P. Spahn, G. P. Hellmann, C. E. Finlayson and J. J. Baumberg, *Adv. Eng. Mater.*, 2013, **15**, 948–953.

225 J. J. Walish, Y. Fan, A. Centrone and E. L. Thomas, *Macromol. Rapid Commun.*, 2012, **33**, 1504–1509.

226 H. Xing, J. Li, J. Guo and J. Wei, *J. Mater. Chem. C*, 2015, **3**, 4424–4430.

227 D. Xu, H. Yu, Q. Xu, G. Xu and K. Wang, *ACS Appl. Mater. Interfaces*, 2015, **7**, 8750–8756.

228 T. Endo and H. Kajita, *IEEJ Trans. Sens. Micromach.*, 2016, **136**, 115–119.

229 Z. Wang, J. Zhang, J. Xie, C. Li, Y. Li, S. Liang, Z. Tian, T. Wang, H. Zhang, H. Li, W. Xu and B. Yang, *Adv. Funct. Mater.*, 2010, **20**, 3784–3790.

230 H. S. Lim, J.-H. Lee, J. J. Walish and E. L. Thomas, *ACS Nano*, 2012, **6**, 8933–8939.

231 Z. Yang, D. Shi, X. Zhang, H. Liu, M. Chen and S. Liu, *RSC Adv.*, 2015, **5**, 69263–69267.

232 X. Hong, Y. Peng, J. Bai, B. Ning, Y. Liu, Z. Zhou and Z. Gao, *Small*, 2013, **10**, 1308–1313.

233 J. Li, Z. Zhang, S. Xu, L. Chen, N. Zhou, H. Xiong and H. Peng, *J. Mater. Chem.*, 2011, **21**, 19267–19274.

234 Z. Yang, D. Shi, M. Chen and S. Liu, *Anal. Methods*, 2015, **7**, 8352–8359.

235 A. M. Ruminski, B. H. King, J. Salonen, J. L. Snyder and M. J. Sailor, *Adv. Funct. Mater.*, 2010, **20**, 2874–2883.

236 Y. Zhang, J. Qiu, R. Hu, P. Li, L. Gao, L. Heng, B. Z. Tang and L. Jiang, *Phys. Chem. Chem. Phys.*, 2015, **17**, 9651–9658.

237 F. Wang, Z. Meng, F. Xue, M. Xue, W. Lu, W. Chen, Q. Wang and Y. Wang, *Trends Environ. Anal. Chem.*, 2014, **3-4**, 1–6.

238 H. Wang and K.-Q. Zhang, *Sensors*, 2013, **13**, 4192–4213.

239 C. Fenzl, T. Hirsch and O. S. Wolfbeis, *Angew. Chem. Int. Ed.*, 2014, **53**, 3318–3335.

240 Q. Li, Q. Zeng, L. Shi, X. Zhang and K.-Q. Zhang, *J. Mater. Chem. C*, 2016, **4**, 1752–1763.

241 K. R. Phillips, G. T. England, S. Sunny, E. Shirman, T. Shirman, N. Vogel and J. Aizenberg, *Chem. Soc. Rev.*, 2016, **45**, 281–322.

242 D. J. Mulder, A. P. H. J. Schenning and C. W. M. Bastiaansen, *J. Mater. Chem. C*, 2014, **2**, 6695–6705.

243 Y. P. Zhang, V. P. Chodavarapu, A. G. Kirk and M. P. Andrews, *Sens. Actuators B*, 2013, **176**, 692–697.

244 M. Giese, L. K. Blusch, M. K. Khan, W. Y. Hamad and M. J. MacLachlan, *Angew. Chem. Int. Ed.*, 2014, **53**, 8880–8884.

245 Y. P. Zhang, V. P. Chodavarapu, A. G. Kirk and M. P. Andrews, Proc. SPIE, 2012, p. 825808.

246 H. Hu, Q.-W. Chen, J. Tang, X.-Y. Hu and X.-H. Zhou, *J. Mater. Chem.*, 2012, **22**, 11048–11053.

247 J. A. Schuller, E. S. Barnard, W. Cai, Y. C. Jun, J. S. White and M. L. Brongersma, *Nat. Mater.*, 2010, **9**, 193–204.

248 F. Cheng, J. Gao, T. S. Luk and X. Yang, *Sci. Rep.*, 2015, **5**, 11045.

249 F. Xia and L. Jiang, *Adv. Mater.*, 2008, **20**, 2842–2858.

250 H. Ge, G. Wang, Y. He, X. Wang, Y. Song, L. Jiang and D. Zhu, *ChemPhysChem*, 2006, **7**, 575–578.

251 J. Wang, Y. Zhang, S. Wang, Y. Song and L. Jiang, *Acc. Chem. Res.*, 2011, **44**, 405–415.

252 J.-N. Wang, R.-Q. Shao, Y.-L. Zhang, L. Guo, H.-B. Jiang, D.-X. Lu and H.-B. Sun, *Chem. Asian J.*, 2012, **7**, 301–304.

253 R. H. Siddique, G. Gomard and H. Hölscher, *Nat. Commun.*,

2015, **6**, 6909.
254 H. K. Raut, V. A. Ganesh, A. S. Nair and S. Ramakrishna, *Energy Environ. Sci.*, 2011, **4**, 3779–3804.
255 H. Sai, T. Matsui, K. Saito, M. Kondo and I. Yoshida, *Prog. Photovolt: Res. Appl.*, 2015, **23**, 1572–1580.
256 L. Cui, Y. Li, J. Wang, E. Tian, X. Zhang, Y. Zhang, Y. Song and L. Jiang, *J. Mater. Chem.*, 2009, **19**, 5499–5502.
257 J. Walia, N. Dhindsa, M. Khorasaninejad and S. S. Saini, *Small*, 2013, **10**, 144–151.
258 S. A. Rinne, F. García-Santamaría and P. V. Braun, *Nat. Photonics*, 2007, **2**, 52–56.
259 K. Zhong, P.-J. Demeyer, X. Zhou, O. Kruglova, N. Verellen, V. V. Moshchalkov, K. Song and K. Clays, *J. Mater. Chem. C*, 2014, **2**, 8829–8836.
260 S. Furumi, H. Fudouzi, H. T. Miyazaki and Y. Sakka, *Adv. Mater.*, 2007, **19**, 2067–2072.
261 G. I. N. Waterhouse, A. K. Wahab, M. Al-Oufi, V. Jovic, D. H. Anjum, D. Sun-Waterhouse, J. Llorca and H. Idriss, *Sci. Rep.*, 2013, **3**, 2849.
262 L. Zhang, E. Reisner and J. J. Baumberg, *Energy Environ. Sci.*, 2014, **7**, 1402–1408.
263 L. Zhang, C.-Y. Lin, V. K. Valev, E. Reisner, U. Steiner and J. J. Baumberg, *Small*, 2014, **10**, 3970–3978.
264 J. K. Kim, J. H. Moon, T.-W. Lee and J. H. Park, *Chem. Commun.*, 2012, **48**, 11939–11941.
265 X. Zheng, S. Meng, J. Chen, J. Wang, J. Xian, Y. Shao, X. Fu and D. Li, *J. Phys. Chem. C*, 2013, **117**, 21263–21273.
266 W. Zhang, M. Anaya, G. Lozano, M. E. Calvo, M. B. Johnston, H. Míguez and H. J. Snaith, *Nano Lett.*, 2015, **15**, 1698–1702.
267 A. Herman, C. Vandenbem, O. Deparis, P. Simonis and J.-P. Vigneron, Proc. SPIE, 2011, p. 80940H.
268 S. Berthier, *Photonique des Morphos*, Springer, Paris, 2010.
269 N. Dushkina and A. Lakhtakia, Proc. SPIE, 2009, p. 740106.
270 F. Schenk, *Int. J. Des. Nat. Ecodyn.*, 2009, **4**, 274–284.
271 F. Schenk and A. R. Parker, *Leonardo*, 2011, **44**, 108–115.
272 C. Park, K. Koh and U. Jeong, *Sci. Rep.*, 2015, **5**, 8340.
273 C. Park, T. Lee, Y. Xia, T. J. Shin, J. Myoung and U. Jeong, *Adv. Mater.*, 2014, **26**, 4633–4638.
274 M. Knoth, G. Miehe and H. Fuess, *Adv. Eng. Mater.*, 2005, **7**, 928–931.
275 Y. C. Ryu, T. G. Kim, G.-S. Seo, J. H. Park, C. S. Suh, S.-S. Park, S.-S. Hong and G. D. Lee, *J. Ind. Eng. Chem.*, 2008, **14**, 213–218.
276 J. G. McGrath, R. D. Bock, J. M. Cathcart and L. A. Lyon, *Chem. Mater.*, 2007, **19**, 1584–1591.
277 M. S. Vlad-Cristea, V. Landry, P. Blanchet and C. Ouellet-Plamondon, *ISRN Nanomater.*, 2013, **2013**, 930236.
278 S.-M. Yang, S.-H. Kim, J. W. Shim and G.-R. Yi, Patent EP 2371908, 2011.
279 S.-H. Kim, S. Y. Lee, G.-R. Yi, D. J. Pine and S.-M. Yang, *J. Am. Chem. Soc.*, 2006, **128**, 10897–10904.
280 N. Koay, I. B. Burgess, T. M. Kay, B. A. Nerger, M. Miles-Rossouw, T. Shirman, T. L. Vu, G. England, K. R. Phillips, S. Utech, N. Vogel, M. Kolle and J. Aizenberg, *Opt. Express*, 2014, **22**, 27750–27768.
281 C. H. Lim, H. Kang and S.-H. Kim, *Langmuir*, 2014, **30**, 8350–8356.
282 C. I. Aguirre, E. Reguera and A. Stein, *ACS Appl. Mater. Interfaces*, 2010, **2**, 3257–3262.
283 O. L. J. Pursiainen, J. J. Baumberg, K. Ryan, J. Bauer, H. Winkler, B. Viel and T. Ruhl, *Appl. Phys. Lett.*, 2005, **87**, 101902.
284 C. E. Finlayson, P. Spahn, D. R. E. Snoswell, G. Yates, A. Kontogeorgos, A. I. Haines, G. P. Hellmann and J. J. Baumberg, *Adv. Mater.*, 2011, **23**, 1540–1544.
285 M. Asano, T. Kuroda, S. Shimizu, A. Sakihara, K. Kumazawa and H. Tabata, Patent US 6326094, 2001.